

# Self-Similar Shocks and Winds in Galaxy Clusters

Yu-Qing Lou<sup>1,2,3, \*</sup>, Yan-Fei Jiang<sup>1†</sup> and Chi-Chuan Jin<sup>1‡</sup>

<sup>1</sup> Department of Physics and Tsinghua Centre for Astrophysics (THCA), Tsinghua University, Beijing, 100084, China;

<sup>2</sup> Department of Astronomy and Astrophysics, the University of Chicago, 5640 South Ellis Avenue, Chicago, IL 60637, USA;

<sup>3</sup> National Astronomical Observatories, Chinese Academy of Sciences, A20, Datun Road, Beijing, 100021, China

Accepted 2008 January 18. Received 2007 December 5; in original form 2007 September 19

## ABSTRACT

A theoretical model framework of spherical symmetry is presented for a composite astrophysical system of two polytropic fluids coupled together by gravity to explore large-scale shocks and flow dynamics in clusters of galaxies or in globular clusters. The existence of such large-scale shocks in clusters of galaxies as inferred by high-resolution X-ray and radio imaging observations implies large-scale systematic flows that are beyond usual static models for clusters of galaxies. Here, we explore self-similar two-fluid flow solutions with shocks for a hot polytropic gas flow in a cluster of galaxies in the presence of a massive dark matter (DM) flow after the initiation of a gravitational core collapse or a central AGN activity or a large-scale merging process. In particular, the possibility of DM shocks or sharp jumps of mass density and of velocity dispersion in dark matter halo is discussed and such DM shocks might be detectable through gravitational lensing effects. To examine various plausible scenarios for clusters of galaxies, we describe three possible classes of shock flows within our model framework for different types of temperature, density and flow speed profiles. Depending upon sensible model parameters and shock locations, the hot ICM and DM halo may have various combinations of asymptotic behaviours of outflow, breeze, inflow, contraction or static envelopes at large radii at a given time. We refer to asymptotic outflows of hot ICM at large radii as the *galaxy cluster wind*. As a result of such galaxy cluster winds and simultaneous contractions of DM halo during the course of galaxy cluster evolution, there would be less hot ICM within clusters of galaxies as compared to the average baryon fraction in the Universe. Physically, it is then expected that such ‘missing baryons’ with lower temperatures reside in the periphery of galaxy clusters on much larger scales. Based on our model analysis, we also predict a limiting (the steepest) radial scaling form for mass density profiles of  $r^{-3}$  within clusters of galaxies.

**Key words:** dark matter — galaxies: clusters: general — gravitation — hydrodynamics — shock waves — X-rays: galaxies: clusters

## 1 INTRODUCTION

Extensive X-ray observations have revealed that almost completely ionized hot gas medium permeates within clusters of galaxies with a typical temperature range of  $\sim 10^7 - 10^8$  K and a range of typical electron number density  $\sim 10^{-2} - 10^{-4} \text{ cm}^{-3}$  (e.g., Cavaliere & Fusco-Femiano 1978; Sarazin 1988; Fabian 1994). Clusters of galaxies are largely gravitationally bound systems on spatial scales of several Mpc; together with the strong evidence of high velocity dispersions of galaxies (e.g.,  $\sim 700 - 1000 \text{ km s}^{-1}$ ), hot X-ray emitting thermal electron gas, and gravitational

lensing effects, we have realized the presence of massive dark matter halo within clusters of galaxies. Physical properties of galaxy clusters with static models of spherical symmetry have been extensively studied in the past (e.g., Lea 1975; Cavaliere & Fusco-Femiano 1976, 1978; Sarazin & Bahcall 1977; Sarazin 1988; Fabian 1994; Carilli & Taylor 2002; Voit 2005).

In the past several years, high-resolution X-ray imaging observations have revealed density, temperature and pressure jumps in the hot intracluster medium (ICM) within clusters of galaxies (e.g., Fabian et al. 2003; Nulsen et al. 2005a; Nulsen et al. 2005b; McNamara et al. 2005), indicating that these structures are likely large-scale shocks rather than cold fronts (e.g., Sanders & Fabian 2006). Active galactic nuclei (AGNs) (e.g., Nulsen et al. 2005a; Nulsen et al. 2005b; McNamara et al. 2005) and merging galaxies (e.g.,

\* Email: louyq@tsinghua.edu.cn; lou@oddsjob.uchicago.edu

† jiangyanfei1986@gmail.com

‡ jcc04@mails.tsinghua.edu.cn

Markevitch & Vikhlinin 2001; Markevitch et al. 2002; Gabici & Blasi 2003; Markevitch et al. 2005) are proposed to be the driving force and energy source of these large-scale shocks. In addition, large-scale sound waves in clusters of galaxies have been proposed by Sanders & Fabian (2007) to explain the observed quasi-concentric ripples in surface brightness of X-ray emissions. Once shocks are identified in clusters of galaxies, there must be large-scale flows involved. In other words, these clusters of galaxies cannot be really static on large scales at least in the spatial region where shocks are presumably identified. Relative to the cluster centre, radial distances of shocks observed vary from tens of kpcs (e.g., McNamara et al. 2005; Nulsen et al. 2005b) to several Mpcs (e.g., A3667 in Rotteringer et al. 1997; A3376 in Bagchi et al. 2006; galaxy clusters A786, A2255, A2256 in Ensslin et al. 1998); at yet smaller radii around the centre, there could be emerging shocks that may not be easily identified. We take the point of view that these shocks are moving in hot ICM and we simply catch them at different epochs of evolution. These shocks may all be born somewhere around the central region and travel outwards to the locations we observe at the present epoch. For those clusters of galaxies without shock signatures, one possibility is that shocks have occurred in the distant past and have disappeared after their energies were dissipated during the process of propagation. So large-scale shocks and flows may well be common phenomena in clusters of galaxies.

On much smaller scales compared to those of clusters of galaxies, X-rays have been also observed in globular clusters (e.g., Verbunt et al. 1984) and these emissions are interpreted by some as associated with flowing gas towards a black hole residing in the centre of globular clusters (e.g., Silk & Arons 1975). Moreover, outflows of gas materials from globular clusters have also been discussed in the literature (e.g., VandenBerg 1978). Fully relaxed globular clusters can be well treated as spherically symmetric (e.g., Harris & Racine 1979). One may view the collection of stars as one ‘fluid’ and the tenuous gas as another fluid; these two fluids are coupled together by gravity on large scales. Here, we note globular clusters in passing and will mainly focus on large-scale self-similar dynamics for clusters of galaxies.

With these two classes of astrophysical systems in mind, we develop a theoretical model framework of spherical symmetry to study dynamic behaviours of hot ICM and dark matter halo using the two-fluid approximation (e.g., Lou 2005), where the two polytropic fluids are coupled together by gravity. We should note that here the notion of a polytropic fluid is fairly general in the sense of specific entropy conservation along streamlines (Lou & Cao 2007).

In the context of large-scale structure formation, extensive numerical works have been carried out to simulate the formation of galaxy clusters in the expanding universe, providing information for the hot ICM and dark matter halo (see, e.g., Bertschinger 1998 for a review on numerical simulations of structure formation in the universe). Evrard (1990) and Thomas & Couchman (1992) simulated properties (such as the number density and temperature profiles) of a hot gas in the presence of a dark matter halo. In Katz & White (1993) and Frenk et al. (1996), the radial cooling process is simulated. In particular, Evrard et al. (1994) simulated the formation of galaxies with two gravitationally coupled fluids representing dark matter halo and

baryon matter, which is similar in essence to the approximation adopted in our semi-analytical model for clusters of galaxies but on much larger scales.

Various self-similar solutions describing hydrodynamic processes of a single self-gravitational isothermal or polytropic gas under spherical symmetry have been investigated previously in contexts of star formation (e.g., Larson 1969a; Larson 1969b; Shu 1977; Hunter 1977; Shu et al. 1987; Lou & Shen 2004). Very recently, asymptotic behaviours of novel quasi-static solutions in a single polytropic gas sphere with self-gravity have been reported by Lou & Wang (2006, 2007) and was utilized to model rebound (MHD) shocks in supernovae (Wang & Lou 2007). For an astrophysical system of two fluids coupled by gravity, we can systematically extend these self-similar solutions, especially the new quasi-static solution, which may be used to describe behaviours of hot ICM and dark matter halo in clusters of galaxies. Except for the gravitational effect in the Newtonian sense, nothing else is known about dark matter particles at present. Using the coupled two-fluid model, we might be able to learn physical properties of dark matter halo through detectable diagnostics of hot ICM and of gravitational lensing effects.

For clusters of galaxies, there is an outstanding problem of ‘missing baryons’. Extensive X-ray observations have indicated that the baryon mass fraction in clusters of galaxies is typically less than the prediction of primordial nucleosynthesis (e.g., Ettori & Fabian 1999; Ettori 2003; He et al. 2005; McGaugh 2007). This discrepancy becomes more difficult to reconcile in the cores of galaxy clusters (e.g., Sand et al. 2003). The best fit of cosmological parameters with tiny temperature fluctuations of the cosmic microwave background (CMB) radiation and large-scale structure clustering shows that relative to the critical mass density  $\rho_c$  in the universe, the mass density of baryon matter is  $\Omega_b = 0.0224 \pm 0.0009 h_{100}^{-2}$  and the total matter density is  $\Omega_m = 0.135_{-0.009}^{+0.008} h_{100}^{-2}$ , where parameter  $h_{100}$  is related to the Hubble constant  $H_0$  by  $H_0 = 100 h_{100} \text{ km s}^{-1} \text{ Mpc}^{-1}$ . Therefore, the mean cosmic baryon mass fraction is  $f_b \equiv \Omega_b / \Omega_m = 0.166_{-0.013}^{+0.012}$  (e.g., He et al. 2005 and references therein). While there are different methods in determining the  $f_b$  value, the cosmic baryon fraction  $f_b$  is around 0.17 (e.g., McGaugh 2007). However in clusters of galaxies, the average gas (baryon) fraction inferred by two methods are about  $0.107_{-0.019}^{+0.028}$  and  $0.111_{-0.063}^{+0.069}$  (e.g., Ettori 2003). Others estimated that the baryon fraction  $f_b$  observed in clusters of galaxies can be lower than the cosmic baryon fraction by about 10%–20% at  $z = 0$  (e.g., He et al. 2005). Some even claimed that the value of  $f_b$  can be lowered by as much as 30% (e.g., Ettori 2003). In conclusion, the baryon fraction in most clusters of galaxies are systematically lower than the average cosmic value  $f_b$  except those highest estimates for gas (baryon) mass fraction in some clusters of galaxies (e.g., A426, A2142, RXJ1350; see Ettori 2003). To resolve this important issue, the notion of Warm-Hot Intergalactic Medium (WHIM) has been introduced (e.g., Cen & Ostriker 1999, 2006; Ettori 2003). In their opinion, the WHIM may actually exist within clusters of galaxies to account for the mass of ‘missing baryons’, yet the WHIM cannot be detected at present because it does not emit X-rays. These results show that a significant fraction ( $\sim 40\% - 50\%$ ) of the baryon component might be found in the form of

WHIM in the temperature range of  $T \sim 10^{5-7}$  K (e.g., Cen & Ostriker 2006).

As will be discussed in more details, this problem of ‘missing baryons’ in our model scenario is a natural consequence of galaxy cluster winds, be it sustained or sporadic or be it stationary or dynamic during the evolution of galaxy clusters. These so-called ‘missing baryons’ are blown away in the form of hot ICM and cool down gradually with time; with relatively low temperatures, they should mostly reside in the periphery of galaxy clusters and spread out in space on much larger scales. Meanwhile, the dark matter halo may contract within clusters of galaxies in our model. Therefore the mass fraction of baryons  $f_b$  (i.e., the mass ratio of total baryons to the total gravitational mass inferred) would be lower than the initial value when a cluster of galaxies was born and started to evolve. The age of galaxy clusters is estimated to fall in the range of  $\sim 10^9 - 10^{10}$  yr (e.g., Fabian 1994). As galaxy cluster winds may have existed since galaxy clusters were born, the timescale of galaxy cluster winds would be comparable to or somewhat less than this estimate. In Section 3, we show a few specific examples of numerical shock flow solutions in our model and estimate the loss of baryons within a timescale of  $\sim 10^9$  yr.

As different behaviours of temperature profiles have been inferred from X-ray observations of galaxy clusters (Markevitch 1996 and Markevitch et al. 2005 for decreasing temperatures with increasing radius; Peres et al. 1998 and Sanders & Fabian 2006 for nearly constant temperatures in several galaxy clusters; McNamara et al. 2005 and Blanton et al. 2001 for increasing temperatures with increasing radius) and electron number densities are observed to fit a power law fairly well (e.g., Peres et al. 1998; Nulsen et al. 2005b), we shall take the specific entropy conservation along streamlines as the equation of state and see how well this may account for the various observed profiles of thermodynamic variables. By properly choosing model parameters in various regimes, we can describe properties of galaxy clusters to a considerable extent.

This paper is structured as follows. The background and motivation of our model development is introduced in Section 1. Section 2 presents in order the basic formulation for the two-fluid model of spherical symmetry involving two polytropic fluids, self-similar transformation, asymptotic solutions at small and large  $x$ , singular surfaces and sonic critical curves, and shock conditions. In Section 3, we show numerical examples of quasi-static solutions for three different situations. The major results are summarized in Section 4. Finally we discuss our model results and numerical solutions in Section 5. Certain mathematical details are contained in Appendices A through G for the convenience of reference.

## 2 MODEL FORMULATION

As theoretical idealization and simplification, a cluster of galaxies is approximated as fully relaxed or virialized and usually modelled as a static equilibrium system in radial force balance with spherical symmetry. However, large-scale shock features as observed in clusters of galaxies reveal the presence of large-scale flows, although these implied large-scale flows may not be directly measurable at this stage. Our main motivation of this model analysis is to provide a

class of dynamic (rather than static or stationary) models for clusters of galaxies with spherical symmetry. We hope to understand a few basic aspects of this dynamic model framework. We have several plausible processes in mind. First, the formation of clusters of galaxies through large-scale gravitational collapse involving dark matter and baryon matter. Secondly, activities of a central AGN (involving accretions of baryon matter as well as dark matter; e.g., Hu et al. 2004) onto supermassive black holes may give rise to a quasi-spherically symmetric component of disturbances on large scales which can evolve into shocks. Thirdly, merging processes may reach a later phase of core confinement such that a large-scale quasi-spherical symmetry may be a sensible approximation; while releasing energy, it takes time for such a dynamic system to relax and adjust itself.

### 2.1 Self-Similar Equations for a Two-Fluid Model

To study dynamic behaviours of visible baryon matter (such as X-ray and radio emissions from the hot ICM) under the joint gravity of both massive dark matter and baryon matter together, we adopt three assumptions for the dark matter halo. First, self-interacting dark matter particle models have been proposed earlier by some researchers (e.g., Carlson et al. 1992; Machacek 1994; Spergel & Steinhardt 2000) to solve the problems encountered by cold dark matter models. Furthermore, properties of collisional dark matter particles (e.g., Ostriker 2000; Hu & Lou 2007) and fluid dark matter (e.g., Peebles 2000; Subramanian 2000; Moore et al. 2000; Hennawi & Ostriker 2002; Lou 2005; Hu et al. 2006) were proposed as an alternative approach to probe DM dynamics. On large scales, one may view high velocity dispersions ( $\sim 700 - 1000$  km s $^{-1}$ ) of DM particles to produce an effective pressure against gravity as described by the Jeans equation (e.g., Binney & Tremaine 1987). In particular, Evrard et al. (1994) numerically simulated formation of galaxies using a model consisting of two gravitationally coupled fluids representing dark matter and baryon matter. While a distribution function approach can be applied to study properties of galaxy clusters, we model a dark matter halo in a ‘fluid’ approximation to simplify the mathematical treatment. On large scales and without resonances, we should be able to understand various dynamic behaviours of hot intracluster medium (ICM) and the dark matter halo in this two-fluid approximation (Lou 2005). Secondly, we assume the two-fluid system of galaxy clusters to be spherically symmetric with a common centre and without rotation for simplicity. On much smaller scales, this simplification would be a very good approximation for globular clusters containing millions of stars and gas. Thirdly, dark matter interacts with hot ICM only through gravity. Based on the above assumptions, we readily write out a set of coupled nonlinear partial differential equations to describe the two-fluid flow system with hot ICM and dark matter halo coupled by gravity. In spherical polar coordinates  $(r, \theta, \phi)$ , the equation for mass conservation is described by

$$\frac{\partial M_i}{\partial t} + u_i \frac{\partial M_i}{\partial r} = 0 \quad \text{and} \quad \frac{\partial M_i}{\partial r} = 4\pi r^2 \rho_i, \quad (1)$$

where  $r$  is radius and  $t$  is time; subscripts  $i = 1, 2$  stand for dark matter halo (fluid 1) and hot ICM (fluid 2), respectively. For simplicity, all variables with a subscript  $i$

denote associations with fluid  $i$ . When referring to a specific fluid  $i$ , we would write out subscripts 1 or 2 explicitly. Here,  $M_i(r, t)$ ,  $\rho_i(r, t)$ , and  $u_i(r, t)$  are respectively the enclosed mass, the mass density, and the radial flow speed at radius  $r$  and time  $t$  for fluid  $i$ . Another familiar form equivalent to the above continuity equation (1) is

$$\frac{\partial \rho_i}{\partial t} + \frac{1}{r^2} \frac{\partial}{\partial r} (r^2 \rho_i u_i) = 0. \quad (2)$$

The Euler radial momentum equation is

$$\frac{\partial u_i}{\partial t} + u_i \frac{\partial u_i}{\partial r} = -\frac{1}{\rho_i} \frac{\partial P_i}{\partial r} - \frac{G(M_1 + M_2)}{r^2}, \quad (3)$$

where  $P_i(r, t)$  is the pressure at radius  $r$  and time  $t$  for fluid  $i$ ;  $M_1$  and  $M_2$  are the enclosed masses of fluid 1 and fluid 2, respectively;  $G = 6.67 \times 10^{-11} \text{ kg}^{-1} \text{ m}^3 \text{ s}^{-2}$  is the gravitational constant.<sup>1</sup> The coupling effect of the two fluids is explicitly contained in the gravity term in equation (3). Finally, we take the conservation equation of specific ‘entropy’ along streamlines as the equation of state (e.g., Fatuzzo et al. 2004; Wang & Lou 2007; Lou & Cao 2007)

$$\left( \frac{\partial}{\partial t} + u_i \frac{\partial}{\partial r} \right) \left( \frac{P_i}{\rho_i^{\gamma_i}} \right) = 0, \quad (4)$$

where  $\gamma_i$  is the polytropic index for fluid  $i$ . In general, polytropic indices  $\gamma_1$  and  $\gamma_2$  are allowed to be different.

Equations (1) – (4) form a set of nonlinear partial differential equations and contain an important subset of nonlinear self-similar solutions with or without shocks. We now introduce a set of self-similar transformation for the two polytropic fluids (e.g., Suto & Silk 1988; Lou & Wang 2006) below

$$x_i = \frac{r}{K_i^{1/2} t^{n_i}}, \quad \rho_i = \frac{\alpha_i(x_i)}{4\pi G t^2}, \quad u_i = K_i^{1/2} t^{n_i-1} v_i(x_i), \\ P_i = \frac{K_i t^{2n_i-4}}{4\pi G} \beta_i(x_i), \quad M_i = \frac{K_i^{3/2} t^{3n_i-2}}{(3n_i-2)G} m_i(x_i), \quad (5)$$

where  $x_i$  is the independent dimensionless similarity variable for fluid  $i$  ( $x_1$  and  $x_2$  are actually related to each other);  $K_i$  is a scale parameter of self-similar transformation for fluid  $i$ ;  $n_i$  is another index parameter of self-similar transformation for fluid  $i$  noted above;  $\alpha_i(x_i)$  is the reduced mass density for fluid  $i$ ;  $v_i(x_i)$  is the reduced radial flow speed for fluid  $i$ ;  $\beta_i(x_i)$  is the reduced pressure for fluid  $i$ ; and  $m_i(x_i)$  is the reduced enclosed mass for fluid  $i$ . All these reduced variables are functions of independent variable  $x_i$  only. In principle, parameter  $n_1$  does not need to be equal  $n_2$ . But equation (3) contains factors like  $t^{n_1}$  and  $t^{n_2}$  at the same time after the self-similar transformation. Therefore in order to obtain the self-similar dimensionless ordinary differential equations (ODEs) in terms of  $x_i$  without involving explicit temporal factors of time  $t$ , we simply require  $n_1 = n_2 = n$  as a single parameter and shall not distinguish the two from now on. With the specific entropy conservation (4) along streamlines, it is not necessary to require  $n = 2 - \gamma_i$  here (e.g., Yahil 1983; Suto & Silk 1988; Lou & Wang 2006, 2007). In fact with  $1 < \gamma_i < 2$ , we shall explore three possible situations of  $2/3 < n < 1$ ,  $n = 1$  and  $n > 1$ , respectively. We note that self-similar processes of galaxy cluster evolution and of cooling

waves in galaxy clusters have also been studied previously (e.g., Bertschinger 1989; Jain & Bertschinger 1996). Here, cooling waves refer to a self-similar expansion of cooling flow region. While the cooling region expands, the hot ICM itself does not move out.

By performing self-similar transformation (5), the reduced enclosed mass  $m_i(x_i)$  can be expressed as (e.g., Suto & Silk 1988; Lou & Wang 2006; Lou & Cao 2007)

$$m_i(x_i) = \alpha_i x_i^2 (n x_i - v_i). \quad (6)$$

Since the enclosed mass  $M_i > 0$ , we should require  $m_i > 0$  and  $n x_i > v_i$  for  $n > 2/3$ , while for  $n < 2/3$ , we require  $m_i < 0$  and  $n x_i < v_i$ ; the latter is generally impossible for semi-complete solutions in the range of  $0^+ < x < +\infty$ . Using equation (6) and self-similar transformation (5), specific entropy conservation (4) along streamlines leads to

$$\frac{\beta_i(x_i)}{\alpha_i^{\gamma_i}(x_i)} = C_{0,i} m_i^{q_i}(x_i), \quad (7)$$

where  $q_i \equiv 2(n + \gamma_i - 2)/(3n - 2)$  is a naturally emerged index parameter and  $C_{0,i}$  is an integration constant for each fluid  $i$ . For  $\gamma_i \neq 4/3$ , we can always effectively combine the two coefficients  $C_{0,i}$  and  $K_i$  into a new single constant coefficient, corresponding to a coefficient rescaling in self-similar transformation (5). The case of a single fluid with  $\gamma = 4/3$  is separately considered by Lou & Cao (2007; see also Goldreich & Weber 1980 and Yahil 1983). It then suffices to consider the equation of state in the form of

$$\frac{\beta_i(x_i)}{\alpha_i^{\gamma_i}(x_i)} = m_i^{q_i}(x_i) \quad (8)$$

for fluid  $i$  with coefficients  $C_{0,i}$  being absorbed without loss of generality. Apparently, there are two linearly related independent variables  $x_1$  and  $x_2$  respectively for the two coupled fluids under consideration. We introduce a convenient ratio  $\kappa \equiv (K_1/K_2)^{1/2}$  such that  $\kappa = x_2/x_1$ . We can then express all dependent variables as functions of  $x_1$  only. From now on, we shall rewrite  $x_1$  as  $x$  for simplicity and thus  $x_2 = \kappa x$ . Now mass and momentum conservation equations (2) and (3) can be straightforwardly cast into the following dimensionless forms of four ODEs, namely

$$(n x - v_1) \frac{d\alpha_1}{dx} - \alpha_1 \frac{dv_1}{dx} = -2 \frac{(x - v_1)}{x} \alpha_1, \quad (9)$$

$$(n-1)v_1 - (n x - v_1) \frac{dv_1}{dx} = \\ -\gamma_1 \alpha_1^{q_1 + \gamma_1 - 2} x^{2q_1} (n x - v_1)^{q_1} \frac{d\alpha_1}{dx} \\ - q_1 \alpha_1^{q_1 + \gamma_1 - 1} x^{2q_1} (n x - v_1)^{q_1 - 1} (3n - 2) \\ - \frac{\alpha_1 (n x - v_1)}{(3n - 2)} - \frac{\alpha_2 (\kappa n x - v_2)}{(3n - 2)\kappa}, \quad (10)$$

$$(\kappa n x - v_2) \frac{d\alpha_2}{dx} - \alpha_2 \frac{dv_2}{dx} = -2 \frac{(\kappa x - v_2)}{x} \alpha_2, \quad (11)$$

$$(n-1)v_2 - \frac{(\kappa n x - v_2)}{\kappa} \frac{dv_2}{dx} = \\ -\frac{\gamma_2}{\kappa} \alpha_2^{q_2 + \gamma_2 - 2} \kappa^{2q_2} x^{2q_2} (\kappa n x - v_2)^{q_2} \frac{d\alpha_2}{dx} \\ - q_2 \alpha_2^{q_2 + \gamma_2 - 1} \kappa^{2q_2} x^{2q_2} (\kappa n x - v_2)^{q_2 - 1} (3n - 2) \\ - \frac{\alpha_2 (\kappa n x - v_2)}{(3n - 2)} - \frac{\kappa \alpha_1 (n x - v_1)}{(3n - 2)}. \quad (12)$$

<sup>1</sup> In Lou & Wang (2006), there is a typo in the unit of  $G$ ; it should be  $\text{cm}^3$  instead of  $\text{cm}^{-3}$ .

After rearrangement and algebraic manipulations of above four equations (9)–(12), the reduced radial flow speeds  $v_1(x)$  and  $v_2(x)$  and the reduced mass densities  $\alpha_1(x)$  and  $\alpha_2(x)$  are then determined equivalently by four coupled first-order nonlinear ODEs shown below.

$$\frac{d\alpha_1(x)}{dx} = \frac{\mathcal{A}_1(x)}{\mathcal{D}_1(x)}, \quad (13)$$

$$\frac{dv_1(x)}{dx} = \frac{\mathcal{V}_1(x)}{\mathcal{D}_1(x)}, \quad (14)$$

$$\frac{d\alpha_2(x)}{dx} = \frac{\mathcal{A}_2(x)}{\mathcal{D}_2(x)}, \quad (15)$$

$$\frac{dv_2(x)}{dx} = \frac{\mathcal{V}_2(x)}{\mathcal{D}_2(x)}, \quad (16)$$

where explicit expressions of denominators  $\mathcal{D}_1(x)$  and  $\mathcal{D}_2(x)$  and numerators  $\mathcal{V}_1(x)$  and  $\mathcal{V}_2(x)$  are shown in Appendix A. This set of nonlinear ODEs contains various types of asymptotic solutions at large and small  $x$ . We mainly focus on two of them, one at large  $x$  and the other at small  $x$ .

## 2.2 Tests of Our Model Formulation

Our model formulation here is sufficiently general and can be readily reduced to various known formulations through various paths of reduction. We indicate these different paths of reduction below to test and confirm the robustness of our approach.

For  $n = 1$  and  $\gamma_1 = \gamma_2 = 1$ , the formulation here reduces to a spherical composite system of two isothermal fluids coupled by gravity as explored by Lou (2005). Static and dynamic models may be constructed in that relatively simple theoretical framework in contexts of clusters of galaxies or of globular clusters but on much smaller scales.

By setting physical variables of one of the two fluids to vanish, the formulation here reduces to that of a single spherical system for a more general polytropic fluid under self-gravity (e.g., Fatuzzo et al. 2004; Lou & Cao 2007; Wang & Lou 2007 in preparation).

If we further set  $n + \gamma = 2$  for a single general polytropic gas under self-gravity, our formulation here reduces to that of a conventional polytropic gas with a constant specific entropy distribution in time and space (Goldreich & Weber 1980; Yahil 1984; Suto & Silk 1988; Lou & Gao 2006; Lou & Wang 2006, 2007).

The single isothermal fluid of spherical symmetry corresponds to  $n = 1$  and  $\gamma = 1$  in our formulation. This problem has been extensively explored in the literature (e.g., Larson 1969a, b; Penston 1969a, b; Shu 1977; Whitworth & Summers 1985; Hunter 1977, 1986; Tsai & Hsu 1995; Shu et al. 2002; Lou & Shen 2004; Shen & Lou 2004; Fatuzzo et al. 2004; Bian & Lou 2005; Yu & Lou 2005; Yu et al. 2006).

Our model is formulated for two gravitationally coupled fluids which are polytropic in the more general sense (see equation 4); this holds the key difference in reference to previous single fluid model under self-gravity with various equations of state. We will show in this section by examples that the solutions similar to the well-known solutions in the single fluid framework (such as the static solution, the central free-fall solution (Shu 1977) and the Larson–Penston

type solution (Larson 1969a, b; Penston 1969a, b)) can also be derived within our model framework.

The static solution in which both flow velocities of the hot gas and dark matter vanish throughout the entire space can be found in our model framework. This is an exact global solution similar to the static solutions with central divergence (i.e., singular isothermal sphere (SIS) and singular polytropic sphere (SPS)) in single fluid model framework (e.g., Shu 1977; Cheng 1978; Lou & Shen 2004; Lou & Wang 2006; Lou & Cao 2007). In our two-fluid model framework, the global static solution (i.e., singular double polytropic spheres (SDPS)) is simply

$$v_1 = v_2 = 0, \quad \alpha_1 = A_1 x^{-2/n}, \quad \alpha_2 = A_2 x^{-2/n}. \quad (17)$$

Here, the two positive density coefficients  $A_1$  and  $A_2$  for two static fluids are readily determined by the following pair of equations

$$\begin{aligned} \frac{n(A_1 + A_2)}{2(3n - 2)} &= (2 - n)n^{q_1 - 1} A_1^{q_1 + \gamma_1 - 1}, \\ \frac{n(A_1 + A_2)}{2(3n - 2)} &= \kappa^{3q_2 - 2} (2 - n)n^{q_2 - 1} A_2^{q_2 + \gamma_2 - 1}, \end{aligned} \quad (18)$$

where  $q_i \equiv 2(n + \gamma_i - 2)/(3n - 2)$  and the ratio  $\kappa$  for the two fluids breaks the symmetry of the above two relations; this symmetry would be explicit for  $\kappa = 1$ . For physical solutions with positive  $A_1$  and  $A_2$ , it is necessary to require  $2/3 < n < 2$ . In other words, both power-law density scalings fall between  $x^{-1}$  and  $x^{-3}$ . For a set of four specified parameters ( $n, \gamma_1, \gamma_2, \kappa$ ), equation (18) does possess sensible real solutions for both coefficients  $A_1 > 0$  and  $A_2 > 0$  and our model then gives a singular static solution for both polytropic fluids simultaneously, i.e., two gravity coupled singular polytropic spheres (SPSs) with divergence of mass densities as  $x \rightarrow 0^+$ . In astrophysical applications, we need to introduce a proper central cutoff.

The LP asymptotic solution and Shu’s central free-fall asymptotic solution were constructed for a single isothermal sphere; in order to get analogous asymptotic solutions in our two-fluid model, we set scaling index parameter  $n = 1$  (defined in self-similar transformation equation (5)) and the polytropic indices of both fluids  $\gamma_1 = 1$  and  $\gamma_2 = 1$ . This is a self-gravitating system of two coupled singular isothermal spheres (Lou 2005).

For two coupled isothermal gas spheres with  $\kappa = 1$ , the generalized version of the Einstein-de Sitter solution (Whitworth & Summers 1985; Shu et al. 2002; Lou & Shen 2004; Lou & Zhai 2007 in preparation) in our model is

$$v_1 = v_2 = 2x/3, \quad \alpha_1 = \alpha_2 = 1/3. \quad (19)$$

This isothermal solution is an exact global solution. For  $\kappa \neq 1$ , this kind of solutions does not exist.

For two coupled conventional polytropic spheres with  $n + \gamma_1 = n + \gamma_2 = 2$  and  $\kappa = 1$ , the generalized version of the Einstein-de Sitter solution of our model is still given by equation (19) (Lou & Wang 2006; Wang & Lou 2007; Lou & Cao 2007).

The asymptotic behaviour when  $x \rightarrow 0^+$  of the solution similar to Shu’s central free-fall asymptotic solution in our model framework is

$$v_1 \rightarrow \mathcal{H}_1 x^{-1/2}, \quad v_2 \rightarrow \mathcal{H}_2 x^{-1/2}, \quad (20)$$

$$\alpha_1 \rightarrow \mathcal{G}_1 x^{-3/2}, \quad \alpha_2 \rightarrow \mathcal{G}_2 x^{-3/2}. \quad (21)$$

Here, the two relations among the four coefficients  $\mathcal{H}_1$ ,  $\mathcal{H}_2$ ,  $\mathcal{G}_1 > 0$  and  $\mathcal{G}_2 > 0$  are

$$\mathcal{H}_1^2 + 2\mathcal{H}_1\mathcal{G}_1 + 2\frac{\mathcal{H}_2\mathcal{G}_2}{\kappa} = 0, \quad (22)$$

$$\mathcal{H}_2^2 + 2\kappa\mathcal{H}_2\mathcal{G}_2 + 2\kappa^2\mathcal{H}_1\mathcal{G}_1 = 0. \quad (23)$$

Therefore, there are only two free coefficients for this kind of central free-fall asymptotic solutions as  $x \rightarrow 0^+$ . The mass at the centre for fluid 1 are determined by  $m_1(0) = -\mathcal{H}_1\mathcal{G}_1$  and the mass at the centre for fluid 2 are determined by  $m_2(0) = -\kappa^2\mathcal{H}_2\mathcal{G}_2$ . Therefore,  $\mathcal{H}_1$  and  $\mathcal{H}_2$  are both negative in equation (20), corresponding to central free-falls of both fluids.

For a polytropic single fluid model, quasi-static asymptotic solutions have been constructed by Lou & Wang (2006). In the next subsection, we will also construct similar quasi-static asymptotic solutions in our two-fluid model and apply the model to the large-scale dynamics of hot gas and dark matter in clusters of galaxies in this paper.

### 2.3 Construction of Two-Fluid Quasi-Static Solutions

As the sound speed of hot ICM in clusters of galaxies is of the order of  $\sim 1000 \text{ km s}^{-1}$  and may decrease towards the centre (such as Abell 2052 in Blanton et al. 2001, and MS0735.6+7421 in McNamara et al. 2005 and in Cavaliere & Fusco-Femiano 1978) while the observed radial flow speed of hot ICM close to the centre is not large, we then construct the quasi-static solution from equations (13)–(16) in the regime of small  $x$  (i.e., parallel to the quasi-static solution of a single fluid of Lou & Wang 2006 and Wang & Lou 2007).<sup>2</sup>

Now we take the static SPS solution (17) and (18) as given in the subsection 2.2 as the leading-order term of the asymptotic quasi-static solution as  $x \rightarrow 0^+$ . Expanding to the second order of this series, the quasi-static solution for two gravity coupled polytropic fluids then takes the form of

$$\begin{aligned} v_1 &\rightarrow L_1 x^k + \dots, \\ v_2 &\rightarrow L_2 x^k + \dots, \end{aligned} \quad (24)$$

$$\begin{aligned} \alpha_1 &\rightarrow A_1 x^{-2/n} + N_1 x^R + \dots, \\ \alpha_2 &\rightarrow A_2 x^{-2/n} + N_2 x^R + \dots, \end{aligned} \quad (25)$$

where  $R \equiv k - 1 - 2/n$  and index parameter<sup>3</sup>  $k$  is determined by the following quartic algebraic equation

$$C_{k,1} k^4 + C_{k,2} k^3 + C_{k,3} k^2 + C_{k,4} k + C_{k,5} = 0. \quad (26)$$

Explicit expressions of the five coefficients ( $C_{k,1}$ ,  $C_{k,2}$ ,  $C_{k,3}$ ,  $C_{k,4}$ ,  $C_{k,5}$ ) can be found in Appendix B. In general, the roots of algebraic quartic equation (26) can be complex. For the higher order terms with respect to static SPS solution, we should require  $Re(k) > 1$  (in static SPS solution (17),

$v_1 = v_2 = 0x$  is regarded as the zeroth order); and the two coefficients  $L_1$  and  $L_2$  are two free parameters with the other two coefficients  $N_1$  and  $N_2$  readily determined by

$$\begin{aligned} N_1 &= \frac{[2(n-1) + nk]A_1 L_1}{(k-1)n^2}, \\ N_2 &= \frac{[2(n-1) + nk]A_2 L_2}{\kappa(k-1)n^2}. \end{aligned} \quad (27)$$

For a complex index parameter  $k$ , please refer to Appendix C for quasi-static solutions with asymptotic oscillations in the regime of small  $x$  (see also Lou & Wang 2006 for quasi-static solutions with asymptotic oscillatory behaviours).

### 2.4 Asymptotic Solutions at Large $x$

In this section, we shall derive asymptotic behaviours of radial flow speed and mass density of the two fluids from equations (13)–(16) as  $x \rightarrow +\infty$ .

The asymptotic series solution at large  $x$  takes the form of

$$\alpha_1(x) \rightarrow E_1 x^{-2/n} + I_1 x^{-3/n} + \dots, \quad (28)$$

$$\alpha_2(x) \rightarrow E_2 x^{-2/n} + I_2 x^{-3/n} + \dots, \quad (29)$$

$$v_1(x) \rightarrow H_1 x^{-1/n+1} + G_1 x^{-2/n+1} + \dots, \quad (30)$$

$$v_2(x) \rightarrow H_2 x^{-1/n+1} + G_2 x^{-2/n+1} + \dots, \quad (31)$$

where  $2/3 < n < 2$  is required and the four coefficients  $E_1$ ,  $E_2$ ,  $H_1$  and  $H_2$  are fairly arbitrary, while the other four coefficients  $I_1$ ,  $I_2$ ,  $G_1$  and  $G_2$  can be expressed in terms of these four arbitrary coefficients (details of these expressions are contained in Appendix D).

For asymptotic radial flow speed solutions (30) and (31), the flow velocities diverge as  $x \rightarrow +\infty$  for  $n > 1$  unless  $H_1 = H_2 = 0$ . For a real astrophysical system, its size is finite; and we may need to introduce a spatial cutoff at a given time in order to make use of these solutions for  $n > 1$  with  $H_1 \neq 0$  and  $H_2 \neq 0$ . For example, the typical size of a galaxy cluster is of the order of several to ten Mpc.

We are certainly interested in finite asymptotic solutions (30) and (31) with  $n = 1$  and  $2/3 < n < 1$ . While for  $n > 1$ , it is possible to set  $H_1 = H_2 = 0$ , and the asymptotic solutions finite at large  $x$  become

$$\alpha_1(x) \rightarrow E_1 x^{-2/n} + F_1 x^{-4/n+1} + \dots, \quad (32)$$

$$\alpha_2(x) \rightarrow E_2 x^{-2/n} + F_2 x^{-4/n+1} + \dots, \quad (33)$$

$$v_1(x) \rightarrow G_1 x^{-2/n+1} + D_1 x^{-4/n+2} + \dots, \quad (34)$$

$$v_2(x) \rightarrow G_2 x^{-2/n+1} + D_2 x^{-4/n+2} + \dots, \quad (35)$$

where  $E_1$  and  $E_2$  are two fairly arbitrary constants and the condition  $n < 2$  is still required;  $G_1$  and  $G_2$  are still defined in Appendix D.  $F_1$ ,  $F_2$ ,  $D_1$ , and  $D_2$  are four constant coefficients of next order expansion terms; these coefficients are determined by specified values of  $E_1$  and  $E_2$  (further details of these coefficient expressions can be found in Appendix D). In principle, we can carry out this series expansion for large  $x$  to the desired order if needed.

<sup>2</sup> Yahil & Ostriker (1973) discussed a steady outflow of gas from galaxy clusters. Their steady wind results show that the gas velocity towards the centre is also very small (see their Fig. 3).

<sup>3</sup> The index parameter  $k$  is taken to be the same for both fluids.

## 2.5 Singular Surfaces and Sonic Critical Curves

The singular surface and sonic critical curve in a single gas flow have been analyzed in details by previous authors (e.g., Suto & Silk 1988; Whitworth & Summers 1985; Lou & Wang 2006; Wang & Lou 2007). For a single gas flow of spherical symmetry, there are smooth solutions going across the sonic critical curve analytically (e.g., Suto & Silk 1988; Whitworth & Summers 1985; Lou & Shen 2004) or with shocks (e.g., Tsai & Hsu 1995; Shu et al. 2000; Bian & Lou 2005; Lou & Wang 2006; Yu et al. 2006; Wang & Lou 2007; Lou & Cao 2007). In our two-fluid model, each fluid component has its own singular surface and sonic critical curve; they are not the same for the two fluids in general and should be treated separately.

The singular surfaces are a set of points when  $\mathcal{D}_1(x) = 0$  for fluid 1 by definition (A5) and  $\mathcal{D}_2(x) = 0$  for fluid 2 by definition (A6). Physically, when the travel speed of disturbances relative to the flow speed is equal to the local sound speed in a fluid, we encounter a singular surface. As there are two fluids in our model, there are two singular surfaces possible for a given set of relevant parameters. The singular surface  $\{x, v_1, \alpha_1\}$  of fluid 1 as defined by  $\mathcal{D}_1(x) = 0$  is then given the following equation

$$(nx - v_1)^2 - \gamma_1 \alpha_1^{q_1 + \gamma_1 - 1} x^{2q_1} (nx - v_1)^{q_1} = 0, \quad (36)$$

and the singular surface  $\{x, v_2, \alpha_2\}$  of fluid 2 as defined by  $\mathcal{D}_2(x) = 0$  is given by a similar equation

$$(\kappa nx - v_2)^2 - \kappa^{2q_2} \gamma_2 \alpha_2^{q_2 + \gamma_2 - 1} x^{2q_2} (\kappa nx - v_2)^{q_2} = 0. \quad (37)$$

Mathematically, sonic critical curves are characteristic lines on the singular surface with the numerators and denominators of self-similar nonlinear ODEs (13) and (14), and (15) and (16) separately being zero simultaneously. The intersection of such two surfaces in  $\{x, v_i, \alpha_i\}$  space gives the sonic critical curve in each fluid  $i$ . As noted above, when the travel speed of disturbances relative to the local flow speed of a specific fluid is equal to the local sound speed, a singularity arises. If one wants to get continuous flow solutions throughout the entire range of  $x$ , such solutions must pass across the singular surface via the sonic critical curves.

In our two-fluid model, as  $\mathcal{V}_1(x)$  and  $\mathcal{A}_1(x)$  contain  $\alpha_2$  and  $v_2$ , we need proper values of  $\alpha_2$  and  $v_2$  in order to determine the sonic critical curve of fluid 1; in reciprocal and in parallel, as  $\mathcal{V}_2(x)$  and  $\mathcal{A}_2(x)$  contain  $\alpha_1$  and  $v_1$ , we need proper values of  $\alpha_1$  and  $v_1$  in order to determine the sonic critical curve of fluid 2. This is a major yet expected difference as compared with the case of a single fluid. Therefore in principle, for a given position of  $x$ , there is a critical point (a point on the critical curve) for fluid  $i$  once a set of  $(\alpha_i, v_i)$  at that  $x$  of the other fluid is given. As the two fluids do not have their critical curves at the same  $x$  in general, there are only two eigendirections for a given set of parameters, which is similar to the case of a single fluid model (Lou & Wang 2006; Wang & Lou 2007). The equations and specific procedure to determine the eigendirections can be found in Appendix E.

In reference to our quasi-static solution for small  $x$ , the condition for the corresponding singular surface  $\mathcal{D}_1(x) = 0$

of fluid 1 has the asymptotic behaviour when  $x \rightarrow 0^+$ :

$$\begin{aligned} nx &= \left( \gamma_1 \alpha_1^{q_1 + \gamma_1 - 1} x^{2q_1} \right)^{1/(2-q_1)} + v_1 \\ &\rightarrow \left[ \gamma_1 A_1^{q_1 + \gamma_1 - 1} \right]^{1/(2-q_1)} x^{1-2/[n(2-q_1)]}. \end{aligned} \quad (38)$$

For  $\mathcal{D}_2(x) = 0$ , the asymptotic behaviour of the corresponding singular surface for fluid 2 when  $x \rightarrow 0^+$  is

$$\begin{aligned} \kappa nx &= \left( \kappa^{2q_2} \gamma_2 \alpha_2^{q_2 + \gamma_2 - 1} x^{2q_2} \right)^{1/(2-q_2)} + v_2 \\ &\rightarrow \left[ \gamma_2 \kappa^{2q_2} A_2^{q_2 + \gamma_2 - 1} \right]^{1/(2-q_2)} x^{1-2/[n(2-q_2)]}. \end{aligned} \quad (39)$$

Therefore if  $1 - 2/[n(2 - q_i)] > 0$ , the corresponding singular surface of fluid  $i$  passes through the origin point ( $x = 0$  and  $v_i = 0$ ); otherwise, it cannot pass the zero point.

When  $x \rightarrow +\infty$ , the asymptotic behaviour of  $\alpha_i(x)$  is (see asymptotic solutions (28), (29), (D9) and (D10)) characterized by  $\alpha_i \rightarrow E_i x^{-2/n} + \dots$ . Then for this same limit of large  $x$ , the singular surface condition  $\mathcal{D}_1(x) = 0$  becomes

$$\begin{aligned} v_1 &= nx - \left( \gamma_1 \alpha_1^{q_1 + \gamma_1 - 1} x^{2q_1} \right)^{1/(2-q_1)} \\ &\rightarrow nx - \left( \gamma_1 E_1^{q_1 + \gamma_1 - 1} \right)^{1/(2-q_1)} x^{1-2/[n(2-q_1)]}. \end{aligned} \quad (40)$$

Since when  $x \rightarrow +\infty$ ,  $v_1(x)$  is either zero or  $v_1 \rightarrow H_1 x^{1-1/n}$  and  $1 - 2/[n(2 - q_1)] \neq 1$  for any values of  $n$  and  $q_1$ , our asymptotic solutions will not lie on the singular surface for fluid 1. For  $\mathcal{D}_2(x) = 0$ , we have the similar result

$$\begin{aligned} v_2 &= \kappa nx - \left( \kappa^{2q_2} \gamma_2 \alpha_2^{q_2 + \gamma_2 - 1} x^{2q_2} \right)^{1/(2-q_2)} \\ &\rightarrow \kappa nx - \left( \gamma_2 \kappa^{2q_2} E_2^{q_2 + \gamma_2 - 1} \right)^{1/(2-q_2)} x^{1-2/[n(2-q_2)]}. \end{aligned} \quad (41)$$

Since when  $x \rightarrow +\infty$ ,  $v_2$  is either zero or  $v_2 \rightarrow H_2 x^{1-1/n}$  and  $1 - 2/[n(2 - q_2)] \neq 1$  for any values of  $n$  and  $q_2$ , our asymptotic solutions will not lie on the singular surface for fluid 2. In summary, for either fluid in the regime of  $x \rightarrow +\infty$ , our asymptotic solutions will not encounter the respective singular surfaces.

## 2.6 Jump Conditions for Self-Similar Shocks

Large-scale shocks have been revealed in clusters of galaxies through high-resolution X-ray imaging observations and radio observations (e.g., Nulsen et al. 2005a, 2005b; McNamara et al. 2005; Bagchi et al. 2006). In order to probe and model such shock features in clusters of galaxies, we construct numerically semi-complete flow solutions with shocks across singular surfaces in both hot gas and dark matter halo separately. These large-scale shocks travel outward in a self-similar manner with asymptotic flow signatures at large  $r$  for given time  $t$ .

In principle, the self-similar form of shock radial positions  $r_{s,i}$  in fluid  $i$  can be expressed either by the downstream parameters ( $K_i$  and  $x_i$  on the downstream side of a shock) or by the upstream parameters ( $K_i$  and  $x_i$  on the upstream side of a shock). For simplicity, we express shock radial positions  $r_{s,i}$  in terms of the upstream parameters. For fluid  $i$ , the shock radial position is denoted by

$$r_{s,i} = K_{u,i}^{1/2} t^n x_{u,i}, \quad (42)$$

where  $K_{u,i}$  is the upstream value of  $K_i$  and  $x_{u,i}$  is the shock

position in terms of the upstream independent self-similar variable for fluid  $i$ . We introduce the sound speed ratio  $\lambda_i$  across a shock for fluid  $i$  as

$$\lambda_i = \left( \frac{K_{d,i}}{K_{u,i}} \right)^{1/2}, \quad (43)$$

where the subscript  $d$  denotes the downstream side (i.e., from the shock position towards the centre) while the subscript  $u$  denotes the upstream side (i.e., from the shock position towards infinity). In reference to a shock,  $K_{d,i}$  is the parameter of  $K_i$  on the downstream side;  $x_{d,i}$  is the shock location in terms of the downstream self-similar variable for fluid  $i$ ;  $\rho_{d,i}$  is the mass density downstream of a shock in fluid  $i$  while  $\alpha_{d,i}$  is the reduced mass density of a shock downstream of fluid  $i$ ;  $P_{d,i}$  is the pressure downstream of a shock for fluid  $i$  while  $\beta_{d,i}$  is the reduced pressure downstream of a shock for fluid  $i$ ;  $u_{d,i}$  is the radial flow speed downstream of a shock for fluid  $i$  while  $v_{d,i}$  is the reduced radial flow speed downstream of a shock for fluid  $i$ ;  $M_{d,i}$  is the enclosed mass downstream of a shock for fluid  $i$  while  $m_{d,i}$  is the reduced enclosed mass downstream of a shock for fluid  $i$ . In one-to-one correspondence, all these variables with subscript  $\{u, i\}$  refer to variables on the upstream side of a shock for fluid  $i$ . In order to construct self-similar shocks, we require index parameter  $n$  to be the same across a shock to avoid unphysical interface separation. As the shock radius is  $r_{s,i} = K_{u,i} t^n x_{u,i}$ , the dimensional shock speed is then given by

$$u_{s,i} = \frac{\partial r_{s,i}}{\partial t} = n K_{u,i}^{1/2} t^{n-1} x_{u,i} = n \frac{r_{s,i}}{t}. \quad (44)$$

Here,  $u_{s,i}$  is the travel speed of a self-similar shock in fluid  $i$ , indicating that the shock actually travels with a variable speed for  $n \neq 1$ . For  $n > 1$  and  $n < 1$ , the shock travel speed increases (acceleration) and decreases (deceleration) with time  $t$ , respectively. For  $n = 1$  and fairly arbitrary  $\gamma_i$ , such a self-similar shock (not necessarily isothermal though) travels with a constant speed. In clusters of galaxies, positions of shocks observed vary from tens of kpcs (e.g., McNamara et al. 2005; Nulsen et al. 2005b) to a few Mpcs (e.g., A3667 in Rotteringer et al. 1997; galaxy cluster Abell 3376 in Bagchi et al. 2006; ZwCl 2341.1+0000 in Bagchi et al. 2002; A786, A2255, A2256 in Ensslin et al. 1998). In our scenario, such shocks actually travel to current positions from a inner region around the cluster centre after their emergence, which can be estimated in our model framework. Then in our scenario at time  $t$ , the shock position  $r_{s,i}$  is determined by the following equation

$$r_{s,i} = C_{s,i} t^n, \quad (45)$$

where  $C_{s,i} \equiv K_{u,i}^{1/2} x_{u,i}$  is a constant to be estimated from observations at a certain time under specific situations.

The self-similar transformation for variables on the downstream side of a shock is

$$x_{d,i} = \frac{r_{s,i}}{\lambda_i K_{u,i}^{1/2} t^n}, \quad (46)$$

$$\rho_{d,i} = \frac{\alpha_{d,i}(x_{d,i})}{4\pi G t^2}, \quad (47)$$

$$P_{d,i} = \lambda_i^2 \frac{K_{u,i} t^{2n-4}}{4\pi G} \beta_{d,i}(x_{d,i}), \quad (48)$$

$$u_{d,i} = \lambda_i K_{u,i}^{1/2} t^{n-1} v_{d,i}(x_{d,i}), \quad (49)$$

$$M_{d,i} = \lambda_i^3 \frac{K_{u,i}^{3/2} t^{3n-2}}{(3n-2)G} m_{d,i}(x_{d,i}). \quad (50)$$

In the shock reference framework, the mass conservation equation across a shock front is

$$\rho_{d,i}(u_{s,i} - u_{d,i}) - \rho_{u,i}(u_{s,i} - u_{u,i}) = 0, \quad (51)$$

which can be rewritten conveniently as

$$[\rho_i(u_{s,i} - u_i)]_u^d = 0; \quad (52)$$

likewise, the radial momentum conservation then gives

$$[P_i + \rho_i(u_{s,i} - u_i)^2]_u^d = 0; \quad (53)$$

and the energy conservation equation leads to

$$\left[ \frac{\rho_i}{2} (u_{s,i} - u_i)^3 + \frac{\gamma_i}{(\gamma_i - 1)} P_i (u_{s,i} - u_i) \right]_u^d = 0, \quad (54)$$

where the pair of brackets denotes the difference of the argument on the downstream (superscript  $d$ ) and upstream (subscript  $u$ ) sides of a shock. As for a single fluid, we now introduce two new variables  $\Gamma_{d,i}$  and  $\Gamma_{u,i}$  below

$$\Gamma_{d,i} \equiv n - v_{d,i}/x_{d,i}, \quad (55)$$

$$\Gamma_{u,i} \equiv n - v_{u,i}/x_{u,i}. \quad (56)$$

Once we know the values of  $(\Gamma, \alpha, x)$  on the downstream side (indicated by a subscript  $d$ ) of a shock, we can immediately calculate the corresponding variables on the upstream side (indicated by a subscript  $u$ ) or vice versa. Details of shock calculations can be found in Appendix F. We only show the major results here. The variable  $\Gamma_{u,i}$  on the upstream side can be computed from the variables on the downstream side from the following equation

$$\Gamma_{u,i} = \frac{2\gamma_i}{(\gamma_i + 1)} \alpha_{d,i}^{q_i + \gamma_i - 1} \Gamma_{d,i}^{q_i - 1} x_{d,i}^{3q_i - 2} + \frac{(\gamma_i - 1)}{(\gamma_i + 1)} \Gamma_{d,i}; \quad (57)$$

other variables can be readily determined in a straightforward manner

$$\alpha_{u,i} = \frac{\alpha_{d,i} \Gamma_{d,i}}{\Gamma_{u,i}}, \quad (58)$$

$$x_{u,i} = \left( \alpha_{d,i}^{q_i + \gamma_i} \Gamma_{d,i}^{q_i} x_{d,i}^{3q_i - 2} + \alpha_{d,i} \Gamma_{d,i}^2 - \alpha_{d,i} \Gamma_{u,i} \Gamma_{d,i} \right)^{1/(3q_i - 2)} \left( \frac{\Gamma_{u,i}^{\gamma_i}}{\alpha_{d,i}^{q_i + \gamma_i} \Gamma_{d,i}^{q_i + \gamma_i}} \right)^{1/(3q_i - 2)}. \quad (59)$$

It then follows that

$$v_{u,i} = x_{u,i}(n - \Gamma_{u,i}) \quad (60)$$

and the ratio  $\lambda_i$  across a shock in fluid  $i$  can be determined accordingly. The upstream Mach number  $\mathcal{M}_{u,i}$  is defined by

$$\begin{aligned} \mathcal{M}_{u,i} &= \frac{(u_{u,i} - u_{s,i})}{a_{u,i}} = \left( \frac{\rho_{u,i}}{\gamma_i P_{u,i}} \right)^{1/2} (u_{u,i} - u_{s,i}) \\ &= \frac{-\Gamma_{u,i}}{\gamma_i^{1/2} \alpha_{u,i}^{(q_i + \gamma_i - 1)/2} x_{u,i}^{q_i - 1} (n x_{u,i} - v_{u,i})^{q_i/2}}, \end{aligned} \quad (61)$$

where  $a_{u,i}$  is the polytropic sound speed on the upstream side of a shock in fluid  $i$ , namely

$$a_{u,i} = \left( \frac{\partial P_{u,i}}{\partial \rho_{u,i}} \right)_s^{1/2} = \left( \frac{\gamma_i P_{u,i}}{\rho_{u,i}} \right)^{1/2}. \quad (62)$$



In general, shock positions in the two fluids are different and the ratio  $\kappa$  will change once either fluid goes across the singular surface via a shock. Right at the shock front, we have  $r_{d,i} = r_{u,i} = r_{s,i}$ ,  $\lambda_i = (K_{d,i}/K_{u,i})^{1/2} = x_{u,i}/x_{d,i}$ ; we can then recalculate  $\kappa$  with the definition  $\kappa \equiv (K_1/K_2)^{1/2} = x_2/x_1$  where  $K_i$  should take the local value.

The specific ‘entropy’ of fluid  $i$  is conserved along streamlines and is given by

$$\begin{aligned} s_i &= c_{v,i} \ln \left( \frac{P_i}{\rho_i^{\gamma_i}} \right) \\ &= c_{v,i} \ln \left\{ K_i^{(4-3\gamma_i)/(3n-2)} \right. \\ &\quad \left. \times (4\pi G)^{\gamma_i-1} [(3n-2)G]^{q_i} M_i^{q_i} \right\}, \end{aligned} \quad (63)$$

where  $c_{v,i}$  is the specific heat capacity at constant volume for fluid  $i$ . As the specific entropy increases from upstream side to downstream side across a shock, either parameter  $K_i$  increases from upstream side to downstream side for  $\gamma_i < 4/3$ , or parameter  $K_i$  decreases from upstream side to downstream side for  $\gamma_i > 4/3$ ; we take  $\gamma_i \neq 4/3$  in this paper. For a single self-gravitating polytropic gas with  $\gamma = 4/3$ , the reader is referred to Lou & Cao (2007) for a further theoretical development of earlier analyses by Goldreich & Weber (1980) and Yahil (1983).

### 3 RESULTS OF NUMERICAL EXAMPLES

Up to now, within the self-similar dynamic model framework of two gravity coupled polytropic fluids, we have successfully constructed the generalized version of quasi-static asymptotic solutions for small  $x$  in reference to the model analysis of Lou & Wang (2006, 2007). This type of self-similar evolution eventually approaches a static configuration with a diverging density towards to the central core region. Meanwhile, we have determined the two singular surfaces and the shock conditions across the two singular surfaces, respectively. In order to construct a global semi-complete quasi-static solution, the relevant parameters required to be known are: the scaling index  $n$  as introduced in self-similar transformation (5); a proper starting value  $x_{ini}$  in the small  $x$  regime to guarantee a reliable numerical integration; the two polytropic indices of dark matter  $\gamma_1$  and of hot ICM  $\gamma_2$  respectively; an estimate of time  $t$  when a self-similar evolution is presumed to begin; the two parameters  $K_1$  and  $K_2$  are related to the sound speeds of two fluids respectively and are introduced in self-similar transformation (5) or equivalently, the parameter  $K_2$  and the ratio  $\kappa \equiv (K_1/K_2)^{1/2}$  of the two fluids; the initial parameters for the quasi-static solution  $L_1$  and  $L_2$  as defined in the quasi-static solution (24); the independent self-similar variables on the downstream sides of shock positions for dark matter  $x_{d,1}$  and for hot ICM  $x_{d,2}$ . Once these eleven parameters are specified, a semi-complete numerical solution can be established. If we just construct a dimensionless solution, then values of  $K_2$  and  $t$  are not needed, indicating that only nine dimensionless parameters are required to be known. Note that parameter  $x_{ini}$  needs to be carefully chosen. Flow parameters at large  $x$  can be determined accordingly.

Now we try to use our two-fluid model to explore dynamic behaviours of hot ICM and dark matter halo for clus-

ters of galaxies. Throughout this paper, we take fluid 1 to represent the dark matter halo and fluid 2 to represent the hot fully ionized ICM. Any variables with subscript 2 are associated with the hot ICM in galaxy clusters in the model analysis. We take the quasi-static solution of both fluids as  $x \rightarrow 0^+$  and go across the singular surfaces with shocks in hot gas and in dark matter halo (at different locations and thus different outward shock travel speeds) respectively. The cluster-scale shocks have been observed in many clusters of galaxies, which may be related to cluster formation processes, central AGN activities or merging of galaxies. Although shocks in a dark matter halo have not yet been detected, there is no obvious reason to rule out this possibility. Observationally, it may be possible to test their presence once the density jump profile of a dark matter halo can be inferred through effects of gravitational lensing. Very recently, Onemli & Sikivie (2007) proposed to interpret certain gravitational lensing observations to be ‘caustics’ (i.e., sharp rises of density in DM halos) in galaxy clusters. While dark matter shocks in our model differ from such DM caustics discussed in the literature, they do share certain similar features and therefore, shocks may also be detected by utilizing gravitational lensing effects. More detailed discussion on DM caustics can be found in the Discussion section at the end. In our model, we can describe various dynamical behaviours of hot ICM when  $r \rightarrow +\infty$ , including inflow, outflow and static solutions. Especially for the outflow solutions at large  $x$ , we shall refer to them as *galaxy cluster winds*, just like solar and stellar winds or galactic winds on much smaller yet different scales. On the basis of galaxy cluster winds and flows of dark matter halo, we will estimate the loss of baryon matter during a timescale of the order of  $\sim 10^9$  yr for the evolution of galaxy clusters.

As scaling index  $n$  is a key parameter controlling asymptotic scaling behaviours of self-similar dynamic solutions, we shall discuss model solutions for three cases of  $2/3 < n < 1$ ,  $n = 1$  and  $n > 1$ , respectively, all with  $\gamma_i$  in the range of  $1 < \gamma_i < 2$  (polytropic indices  $\gamma_1$  and  $\gamma_2$  of two fluids are allowed to be different in general). We use the standard fourth-order Runge-Kutta numerical scheme (e.g., Press et al. 1986) to integrate coupled nonlinear ODEs (13), (14), (15) and (16) with relevant asymptotic solutions in both regimes of large and small  $x$ . As the analytic quasi-static solution is adopted for  $x \rightarrow 0^+$  in this model consideration, we start the numerical integration with an assigned value of  $x_{ini}$ , which is small enough.<sup>4</sup> The corresponding initial values of  $\alpha_i(x)$  and  $v_i(x)$  are determined by quasi-static solution (25) and (24) with mutually consistent coefficients. Once a fluid component encounters its singular surface, we let the fluid go across it via a shock; there is a certain degree of freedom in choosing shock location and thus shock speed in constructing solutions. If the solution can be integrated to infinity (a sufficiently large  $x$  in practice), a semi-complete solution is then obtained in our two-fluid model. Note that in order to avoid unstable numerical integration from small  $x$  outwards, we need to take some appropriate initial parameters and carefully check characteristic features of a true quasi-static solution at small  $x$ .

<sup>4</sup> The rule of thumb criterion for a sensible choice of  $x_{ini}$  is that  $v_i(x)/x^k$  remains constant for a certain range of small  $x$ .

In applications to clusters of galaxies, the virial radius corresponds to the radius where the mass density of dark matter is 200 times of the critical density  $\rho_c$  in the Universe (e.g., Navarro et al. 1996). We follow this convention and denote the virial radius by  $r_{200}$ . Here, the critical mass density  $\rho_c$  is defined by

$$\rho_c = 3H_0^2/(8\pi G), \quad (64)$$

where  $H_0$  is the Hubble constant and  $G = 6.67 \times 10^{-11} \text{ kg}^{-1}\text{m}^3 \text{ s}^{-2}$  is the gravitational constant. Recent *Wilkinson Microwave Anisotropy Probe (WMAP)* results showed a Hubble constant  $H_0 = 72 \pm 8 \text{ km s}^{-1} \text{ Mpc}^{-1}$  (e.g., Freedman et al. 2001; Spergel et al. 2003). Thus the critical mass density is currently inferred to be  $\rho_c = 9.7 \times 10^{-27} \text{ kg m}^{-3}$ . In our discussion on clusters of galaxies, the radius  $r$  will be expressed in unit of the virial radius  $r_{200}$ .

### 3.1 Ranges of $K_2$ and $t$ Values

Once values<sup>5</sup> of  $K_2$  and time  $t$  are chosen in our two-fluid model, we can then simulate a dynamic shock flow of hot ICM in clusters of galaxies under the gravitational influence of a flowing dark matter halo. Physically, we may take  $t$  to be the timescale when a large-scale shock has emerged. As shocks in clusters of galaxies may be initiated by gravitational core collapses or AGN activities or merging galaxies and the timescale for the recurrence of AGNs is of the order of  $\sim 10^8 \text{ yr}$  (or equivalently  $\sim 2 \times 10^{15}$  to  $2 \times 10^{16} \text{ s}$ , e.g., Fabian 1994), we may choose time  $t$  of this magnitude order in our model applications to clusters of galaxies. According to dimensionless equation of state (8) and self-similar transformation (5), we have

$$K_2 = \left[ \frac{\rho_2^{\gamma_2}}{P_2} M_2^{q_2} (4\pi)^{\gamma_2-1} G^{q_2+\gamma_2-1} (3n-2)^{q_2} \right]^{2/(3q_2-2)}. \quad (65)$$

For a hot ICM, we simply apply the ideal gas law  $P_2 = \mathcal{N}_2 k_B T_2$ , where  $\mathcal{N}_2$  is the particle number density,  $k_B$  is the Boltzmann constant,  $P_2$  is the thermal pressure of ICM, and  $T_2$  is the ICM temperature. Then equation (65) appears as

$$K_2 = \left[ \frac{\rho_2^{\gamma_2}}{\mathcal{N}_2 k_B T_2} M_2^{q_2} (4\pi)^{\gamma_2-1} \times G^{q_2+\gamma_2-1} (3n-2)^{q_2} \right]^{2/(3q_2-2)}. \quad (66)$$

As in clusters of galaxies the electron number density is typically  $10^{-2} \sim 10^{-4} \text{ cm}^{-3}$  (e.g., Fabian 1994; Cavaliere & Fusco-Femiano 1978; Nulsen et al. 2005b) and the gas mainly consists of protons, electrons, and  $\alpha$  particles (nuclei of helium atoms), the particle number density is also of this magnitude. The mean molecular weight for ICM in galaxy clusters is about 0.6 g/mol (e.g., Cavaliere & Fusco-Femiano 1978) and the mass of hot ICM in galaxy clusters is of the order of  $10^{13} M_\odot$  (e.g., Peres et al. 1998). Typically, the ICM temperature  $T_2$  varies in the range of  $\sim 10^7 - 10^8 \text{ K}$  (e.g., Fabian 1994). For an observational input of these different parameters, we can then estimate the typical range of  $K_2$

**Table 1.** Values of  $K_2$  in SI unit for different sets of model parameters. We take the mean molecular weight of the typical ICM in galaxy clusters to be 0.59 g/mol, corresponding to the total mass ratio of protons to  $\alpha$  particles being 3. Then the ICM mass density  $\rho_2$  can be calculated from  $N_e$ , the electron number density in the hot ICM, and  $K_2$  is calculated from equation (66). The temperature  $T_2$  is in unit of keV and the electron number density  $N_e$  is in unit of  $\text{cm}^{-3}$ . The enclosed mass  $M_2$  for ICM is in unit of  $10^{13} M_\odot$  ( $M_\odot$  is the solar mass). All values of  $K_2$  in Table 1 are in SI unit.

$n$	$\gamma_2$	$T_2$	$N_e$	$M_2$	$K_2$
0.8	1.31	6	0.004	1	$1.11 \times 10^{21}$
0.8	1.31	7	0.004	1	$2.68 \times 10^{21}$
0.8	1.31	7	0.008	1	$7.84 \times 10^{20}$
1	1.405	8	0.002	1	$3.72 \times 10^8$
1	1.405	7	0.002	1	$6.93 \times 10^8$
1	1.405	8	0.001	2	$1.37 \times 10^9$
1.07	1.42	5	0.001	1	$9.29 \times 10^6$
1.07	1.42	6	0.001	1	$3.98 \times 10^6$
1.07	1.42	6	0.003	1	$3.41 \times 10^7$

values (in SI unit). To be specific, we estimate relevant parameters for our two-fluid model calculations and the results are summarized in Table 1 above.

### 3.2 The ICM Temperature Profile

According to the ideal gas law  $P_2 = \rho_2 k_B T_2 / \mu_0$ , where  $\mu_0$  is the mean molecular mass,  $k_B$  is the Boltzmann constant and  $\rho_2$  is the ICM mass density, the ICM temperature  $T_2$  in our self-similar flow model is given by

$$T_2(r, t) = \frac{\mu_0 K_2}{k_B} t^{2n-2} \kappa^{2q_2} \alpha_2^{q_2+\gamma_2-1} x^{2q_2} (\kappa n x - v_2)^{q_2}. \quad (67)$$

For  $x \rightarrow 0^+$ , the asymptotic behaviour of ICM temperature is then

$$T_2 \rightarrow \frac{\mu_0 K_2}{k_B} t^{2n-2} \kappa^{3q_2} A_2^{q_2+\gamma_2-1} n^{q_2} x^{2-2/n} + \dots, \quad (68)$$

which diverges as  $r \rightarrow 0^+$  for  $n < 1$ . As the radial flow speed  $v_i(x)$  is small compared with  $x$  as  $x \rightarrow +\infty$  (see equations (30), (31), (D11), (D12)) and the reduced mass density  $\alpha_i(x)$  has similar asymptotic scaling behaviours at both large and small  $x$  (see equations (28), (29) and (25)), the ICM temperature  $T_2$  has the similar asymptotic scaling behaviours at both large and small  $x$  because  $T_2$  is closely related to thermodynamic variables  $P_2$  and  $\rho_2$  as well as the enclosed mass  $M_2$ . Therefore for  $n < 1$ , the ICM temperature  $T_2$  decreases with increasing radius  $r$ ; in the limit of  $n \rightarrow (2/3)^+$ , the limiting temperature scaling would be  $\sim r^{-1}$ . In fact, qualitatively similar temperature profiles have been observed in several galaxy clusters (e.g., galaxy clusters A2256, A2319, A665 in Markevitch 1996; and galaxy cluster A520 in Markevitch et al. 2005). Both temperature and mass density diverge as  $x \rightarrow 0^+$  for  $n < 1$ ; we need to introduce a sensible reference radius to cutoff around the cluster centre.

With  $n = 1$ , expression (68) for ICM temperature  $T_2$  remains constant for a certain radial distance around the centre. This kind of solution actually represents galaxy clusters with roughly constant temperature. This kind of galaxy

<sup>5</sup> As an example, we take  $K_2 \equiv K_{d,2}$  in this subsection for the hot ICM on the downstream side of an ICM shock.

clusters has also in fact been observed, such as galaxy cluster A2204 in Peres et al. (1998) and galaxy clusters A2199 and 2A 0335+096 in Sanders & Fabian (2006). For the  $n = 1$  case of our two-fluid model, solutions are not ‘isothermal’ in general because  $\gamma_i \neq 1$ ; and this clearly differs from previous isothermal analyses with  $n = 1$  and  $\gamma = 1$  (e.g., Tsai & Hsu 1995; Lou & Shen 2004; Lou 2005; Bian & Lou 2005). Of course, we could set  $\gamma_1 = 1$  and  $\gamma_2 \neq 1$  for an ‘isothermal’ dark matter flow and a nonisothermal gas or vice versa or  $\gamma_1 = \gamma_2 = 1$  for two ‘isothermal’ flows and so forth. In particular, we emphasize that this  $n = 1$  case fundamentally differs from the condition  $n = 1$  in Suto & Silk (1988), because their specific entropy is not conserved along streamlines with  $n = 1$ .

For  $n > 1$ , the ICM temperature  $T_2$  increases with increasing radius as indicated by expressions (67) and (68). Temperature profiles in many clusters of galaxies do appear to behave in this manner qualitatively in a certain radial range, such as galaxy clusters Ms0735.6 + 7421 (e.g., McNamara et al. 2005), Perseus (e.g., Sanders & Fabian 2007) and A2052 (e.g., Blanton et al. 2001).

### 3.3 Energetics of the Coupled Two-Fluid System

Parallel to the single flow system of an isothermal gas (e.g., Tsai & Hsu 1995), the energy of our coupled polytropic two-fluid system consists of three parts, namely, the gravitational potential energy denoted by  $E_{grav}$ , the kinetic energy of two fluids denoted by  $E_{k,i}$  and the thermal energy of two fluids denoted  $E_{th,i}$ , where the subscript  $i = 1, 2$  refer to fluid 1 (dark matter) and fluid 2 (hot ICM) respectively. In conventional scenarios, AGN activities are sustained by accretions of baryon matter onto a supermassive black hole (SMBH). Conceptually, it is also physically sensible to think of accretions of both baryon matter and dark matter onto a SMBH for AGN activities (e.g., Hu et al. 2006), although only radiations from ICM can directly reach us. Therefore in addition to radiative losses from electrons we observe, the outburst energy of an AGN should also involve the energies associated with hot gas and dark matter. The energy within the shock radius contains the outburst energy of AGN and the original energy in the system prior to an AGN. We may calculate the energy within the shock radius to estimate the order of the outburst energy released by an AGN.

The gravitational energy of our coupled two-fluid system within a radial range between  $r_{min}$  and  $r_{max}$  (the respective dimensionless self-similar variables are  $x_{min}$  and  $x_{max}$  for a specified time  $t$ ) is simply given by

$$E_{grav} = - \int_{r_{min}}^{r_{max}} \frac{G(M_1 + M_2)}{r} (\rho_1 + \rho_2) 4\pi r^2 dr . \quad (69)$$

With self-similar transformation (5), we then derive

$$E_{grav} = - \frac{\kappa^5 K_2^{5/2} t^{5n-4}}{(3n-2)G} \times \int_{x_{min}}^{x_{max}} x^3 \left[ \alpha_1 (nx - v_1) + \alpha_2 \left( nx - \frac{v_2}{\kappa} \right) \right] (\alpha_1 + \alpha_2) dx , \quad (70)$$

where  $x \equiv x_1$  for dark matter halo. The kinetic energy for fluid  $i$  within the radial range between  $r_{min,i}$  and  $r_{max,i}$  (the respective dimensionless self-similar variables are  $x_{min,i}$  and

$x_{max,i}$  for a specified time  $t$ ) is simply given by

$$\begin{aligned} E_{k,i} &= \int_{r_{min,i}}^{r_{max,i}} \frac{\rho_i u_i^2}{2} 4\pi r^2 dr \\ &= \frac{K_i^{5/2} t^{5n-4}}{2G} \int_{x_{min,i}}^{x_{max,i}} \alpha_i v_i^2 x_i^2 dx_i . \end{aligned} \quad (71)$$

The thermal energy of fluid  $i$  within the same radial range of  $r_{min,i}$  and  $r_{max,i}$  is simply given by

$$\begin{aligned} E_{th,i} &= \int_{r_{min,i}}^{r_{max,i}} \frac{\gamma_i P_i}{(\gamma_i - 1)} 4\pi r^2 dr \\ &= \frac{\gamma_i K_i^{5/2} t^{5n-4}}{(\gamma_i - 1)G} \int_{x_{min,i}}^{x_{max,i}} x_i^2 \alpha_i^{\gamma_i} m_i^{q_i} dx_i . \end{aligned} \quad (72)$$

As the polytropic sound speed  $a_i$  in fluid  $i$  is

$$a_i = \left( \gamma_i \frac{P_i}{\rho_i} \right)^{1/2} = \left( \gamma_i \frac{\beta_i}{\alpha_i} \right)^{1/2} K_i^{1/2} t^{n-1} , \quad (73)$$

the common dimensional coefficient in integrals (70)–(72) can be expressed in terms of the sound speed as

$$\frac{K_i^{5/2} t^{5n-4}}{G} = \frac{a_i^5 t}{G} \left( \gamma_i \frac{\beta_i}{\alpha_i} \right)^{-5/2} . \quad (74)$$

In our model, the sound speed  $a_i$  is not a constant, which differs from the isothermal model of Tsai & Hsu (1995) for a single gas.

The total energy of the two-fluid system within the radial range between  $r_{min}$  and  $r_{max}$  is then

$$E_{total} = E_{grav} + \sum_{i=1}^2 E_{k,i} + \sum_{i=1}^2 E_{th,i} . \quad (75)$$

At a certain reference time  $t_1$ , we can calculate the total energy  $E_{total,o}$  within a radial range between  $r_{min}$  and  $r_{max}$ , where neither shock arrives. After a certain time lapse  $t_2$  when both shocks have passed through the radial range under consideration, we can calculate the total energy  $E_{total,f}$  within the same radial domain. Then the energy difference  $E_{total,f} - E_{total,o}$  is the energy input from shock flow. Furthermore, the mean input power during this time interval  $t_2 - t_1$  can be estimated by

$$\mathcal{P}_{total} = (E_{total,f} - E_{total,o}) / (t_2 - t_1) . \quad (76)$$

In addition to radiation losses from the central region, this mean input power can be used to estimate the power from AGN activities. In our model framework, the total energy includes several parts. The X-ray luminosity of galaxy clusters inferred by observations (e.g., Nulsen et al. 2005a; Gizani & Leahy 2004) should come from the thermal energy part of hot ICM. In the estimated outburst energies of AGNs with certain models (e.g, Nulsen et al. 2005a; Gizani & Leahy 2004), only the fraction of energy transmitted to the thermal reservoir of hot ICM is considered. In our scenario, the part of released energy from AGNs is also transmitted to the dark matter as well as the gravitational and kinetic energies of hot ICM. Therefore, our mean power and energy are more than just the thermal energy input to hot ICM.

### 3.4 Solution Examples of $2/3 < n < 1$

In this case of  $2/3 < n < 1$ , features of our global semi-complete solutions are summarized as follows. When  $x \rightarrow$

$+\infty$ ,  $v_i(x)$  goes to zero with a  $\alpha_i(x)$  scaling of  $x^{-2/n}$ . In the other limit of  $x \rightarrow 0^+$ ,  $v_i(x)$  goes to zero with a  $\alpha_i(x)$  scaling of  $x^{-2/n}$ . At large  $x$ , both fluids may have various combinations of asymptotic behaviours of outflow, breeze, static envelope, contraction, inflow as the two shock positions (or outgoing speeds) vary. Through numerical exploration, we note that as the shock position decreases from the vicinity of the singular surface to smaller  $x$  in fluid  $i$ , the corresponding outflow speed  $v_i(x)$  at large  $x$  tends to decrease. If the shock position is reduced further, the fluid at large  $x$  may become static and then turn into a contraction or an inflow. As implied by the limit of our parameter regime for scaling index  $n$ , the most steep density scaling both at large and small  $x$  would be  $\sim x^{-3}$  (Wang & Lou 2007). This limiting density scaling can be systematically tested against observations of galaxy clusters.

Here, we offer a few solution examples with the set of parameters  $\{n, \gamma_1, \gamma_2, \kappa\} = \{0.8, 1.3, 1.31, 0.02\}$ . The two coefficients  $A_1$  and  $A_2$  can be readily calculated from equation (18) and the value of index  $k$  is determined by quartic equation (26) (we choose the root  $k > 1$  for the consistency of series expansion analysis); their specific values are  $\{A_1, A_2, k\} = \{1.76, 0.35, 1.99\}$  correspondingly. For different initial values and shock positions, the global semi-complete solutions for radial flow speeds  $v_i(x)$  (scaled for a clear presentation) are shown in Figures 1 and 2; numerical values of the relevant solution parameters are listed in Table 2. In short, for these four numerical solutions 1, 2, 3 and 4, the nine parameters to determine a dimensionless solution are:  $\{n, \gamma_1, \gamma_2, \kappa, L_1, L_2, x_{ini}, x_{d,1}, x_{d,2}\} = \{0.8, 1.3, 1.31, 0.02, 0.06, -0.00638, 6 \times 10^{-9}, 342, 0.55\}$  for solution 1;  $\{n, \gamma_1, \gamma_2, \kappa, L_1, L_2, x_{ini}, x_{d,1}, x_{d,2}\} = \{0.8, 1.3, 1.31, 0.02, 0.06, -0.00638, 6 \times 10^{-9}, 1.8, 0.63\}$  for solution 2;  $\{n, \gamma_1, \gamma_2, \kappa, L_1, L_2, x_{ini}, x_{d,1}, x_{d,2}\} = \{0.8, 1.3, 1.31, 0.02, -0.673, 0.0716, 6.8 \times 10^{-10}, 0.35, 50\}$  for solution 3;  $\{n, \gamma_1, \gamma_2, \kappa, L_1, L_2, x_{ini}, x_{d,1}, x_{d,2}\} = \{0.8, 1.3, 1.31, 0.02, -0.0051, 0.000542, 1.6 \times 10^{-8}, 0.8, 5\}$  for solution 4. It should be noted that parameter  $x_{ini}$  is not intrinsic to the physical description but must be properly chosen within a certain range for reliable numerical solutions matched with quasi-static asymptotic solutions at small  $x$ .

Solutions such as example solution 2 catch our special attention. Such solutions demonstrate a possible scenario that when  $x \rightarrow +\infty$ , the hot ICM represented by fluid 2 can flow outward while the dark matter halo represented by fluid 1 gradually contracts. As the dark matter halo dominates in clusters of galaxies in terms of mass (the enclosed mass ratio of dark matter halo to hot ICM varies from 4 to 10 in typical clusters of galaxies, e.g., Peres et al. 1998), one can readily understand the behaviour of this kind of dynamic solutions. Since the hot gas in this solution can overcome the overall gravity (dark matter and hot ICM together) and flow outward at large distance, we naturally refer to such gas outflow as the *galaxy cluster wind*. The driving energy of the galaxy cluster wind may come from the gravitational core collapses or AGN activities or merging of galaxies around the centre of galaxy clusters; a self-similar phase gradually emerges after a while of dynamic evolution. For  $x \rightarrow 0^+$ , the flow velocity of dark matter halo is outward. The outflow of dark matter may be propelled by violent outbursts of energy around the cluster centre occurred at earlier times.

In fact, hydrodynamic models for clusters of galaxies

**Table 2.** Parameters for numerical solutions 1, 2, 3 and 4 presented in Figures 1 and 2 with  $2/3 < n < 1$ . In the first column on the left, ‘No.’ is the numeral label to distinguish different example solutions 1, 2, 3 and 4. ‘Type 1’ is the type of flow solutions of fluid 1 when  $x \rightarrow +\infty$ , and ‘Type 2’ is the type of flow solutions of fluid 2 when  $x \rightarrow +\infty$ . Here,  $x_{d,1}$  and  $x_{d,2}$  are the independent self-similar variables on the downstream sides of shock positions for fluids 1 and 2, respectively. Parameters  $E_1$  and  $E_2$  are respectively the coefficients of  $\alpha_1(x)$  and  $\alpha_2(x)$  at a large enough  $x$  according to asymptotic solutions (28) and (29). Parameters  $H_1$  and  $H_2$  are respectively the velocities  $v_1(x)$  of fluid 1 and  $v_2(x)$  of fluid 2 at a large enough  $x$  according to asymptotic solutions (30) and (31). Parameter  $x_{ini}$  is the initial value of  $x$  for a numerical integration. As this table is too long horizontalwise, we break the table in two parts and stack them together.

No.	Type 1	Type 2	$L_1$	$L_2$	$x_{ini}$
1	outflow	outflow	0.06	-0.00638	$6 \times 10^{-9}$
2	inflow	outflow	0.06	-0.00638	$6 \times 10^{-9}$
3	outflow	inflow	-0.673	0.0716	$6.8 \times 10^{-10}$
4	inflow	inflow	-0.0051	0.000542	$1.6 \times 10^{-8}$
$x_{d,1}$	$x_{d,2}$	$E_1$	$E_2$	$H_1$	$H_2$
342	0.55	$6.04 \times 10^5$	0.432	1471	178
1.8	0.63	2.2	0.21	-0.13	0.034
0.35	50	6.22	877	48.5	-7.61
0.8	5	6.99	2.67	-3.44	-0.0269

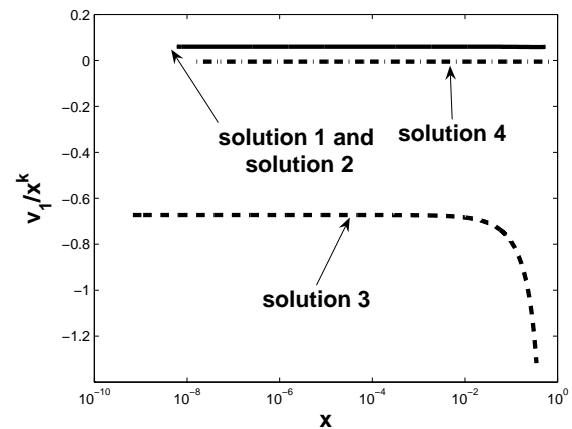


**Figure 1.** Scaled radial flow velocity of fluid 1 (dark matter halo) at small  $x$  with  $2/3 < n < 1$ . The relevant model parameters are summarized in Table 2 for solutions 1, 2, 3 and 4. Note that for a certain range of initial distance,  $v_1(x)/x^k$  remains a constant, showing that these solutions for  $v_1(x)$  are indeed quasi-static for small  $x$ . For all these solutions 1, 2, 3 and 4, we have the same  $\{n, \gamma_1, \gamma_2, \kappa\} = \{0.8, 1.3, 1.31, 0.02\}$ . Solutions 1 and 2 (heavy solid line) coincide in the regime of small  $x$ . The corresponding solution behaviours of  $v_2(x)/x^k$  (for the hot ICM) are shown in Fig. 2.

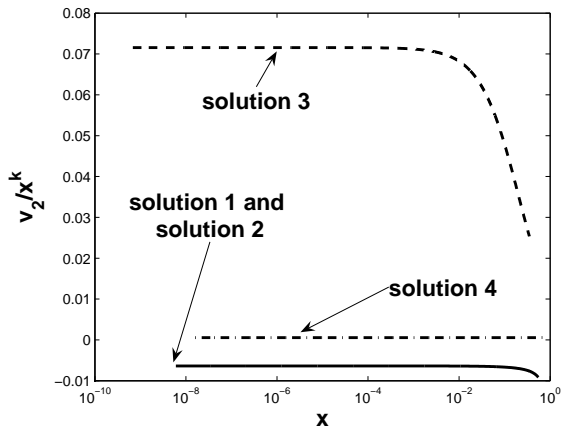


**Figure 2.** Scaled radial flow velocities of fluid 2 (hot ICM) at small  $x$  with  $2/3 < n < 1$ ; the relevant model parameters are listed in Table 2. Note that for a certain range of initial distance,  $v_2(x)/x^k$  remains constant, showing that these solutions 1, 2, 3 and 4 for  $v_2(x)$  are indeed quasi-static for small  $x$ . Together with Figure 1 for fluid 1 (dark matter halo), we have succeeded in constructing solutions with both fluids being quasi-static at small  $x$ . For all these solutions 1, 2, 3 and 4, we have the same  $\{n, \gamma_1, \gamma_2, \kappa\} = \{0.8, 1.3, 1.31, 0.02\}$ . Solutions 1 and 2 (heavy solid line) coincide in the regime of small  $x$ .

have been proposed earlier. In Gunn & Gott (1972), a theory of infall of materials into clusters of galaxies was developed and they applied it to the growth of galaxy clusters and the generation of hot ICM. Bertschinger (1989) discussed the time-dependent evolution of cooling flows in clusters of galaxies and emphasized that although the size of a cooling flow region will increase with time, the gas material itself does not go outward; this mechanism is referred to as ‘cooling waves’. In particular, steady winds from a galaxy clusters (e.g., the Coma cluster) have been discussed by Yahil & Ostriker (1973). Their result indicates a mass loss rate of  $\sim 10^3 - 10^4 M_\odot$  per year. Their model considered a steady-state wind without involving shocks. In our dynamic model, we can construct self-similar solutions such as solution 2 to explore the dynamics of galaxy cluster winds with shocks and possible physical consequences.

For quasi-static solution 2 in small  $x$  shown in Figures 1 and 2, we adopt estimates for the physical parameters  $t = 7.59 \times 10^{15}$  s and  $K_2 = 5.50 \times 10^{20}$  SI unit on the downstream side of the ICM shock. In this example, the shock position in the hot gas is  $r_{s,2} = 48.38$  kpc (shock positions vary from tens of kpc to hundreds of kpc in clusters of galaxies and a similar shock position has been observed in the Perseus cluster; e.g., Fabian et al. 2006). We only apply our model to radii less than several Mpc, say  $\sim 3$  Mpc (e.g., the size scale of the Hydra A cluster is  $\sim 3$  Mpc; see e.g., Taylor et al. 1990). The corresponding flow velocity profiles are displayed in Figure 3 and the profile of electron number density  $N_e$  is displayed in Figure 4. In order to get the electron number density, we take the mean molecular weight to be  $\sim 0.59$  g/mol (see Cavaliere & Fusco-Femiano 1978). In this example, the radial outflow velocity of hot gas at 3Mpc is  $\sim 202$  km  $s^{-1}$  while the radial inflow velocity of dark matter halo at 3Mpc is  $\sim 20.3$  km  $s^{-1}$ . The analytical expression for the polytropic sound speed ratio can be found

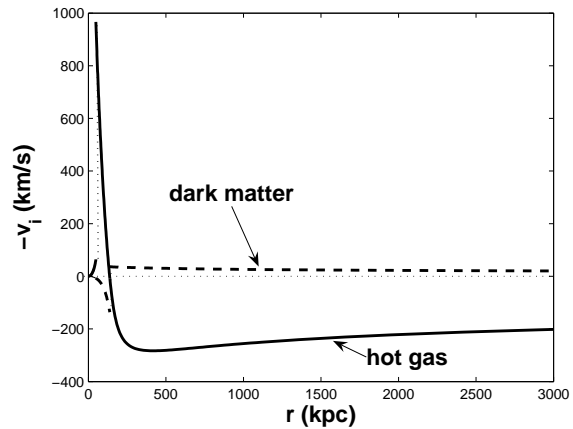


**Figure 3.** Negative radial flow velocities of hot ICM (solid curve) and dark matter halo (dashed curve) of solution 2 with  $t = 7.59 \times 10^{15}$  s and  $K_2 = 5.50 \times 10^{20}$  SI unit on the downstream side of a shock in hot ICM. The shock position in the hot ICM is at  $\sim 48.38$  kpc while the shock position of dark matter is at  $\sim 138.23$  kpc. The initial parameters for the numerical integration are listed in Table 2 (see those for solution 2). The corresponding radial flow velocities at small  $x$  of this solution are shown in Figs. 1 and 2 (solution 2).

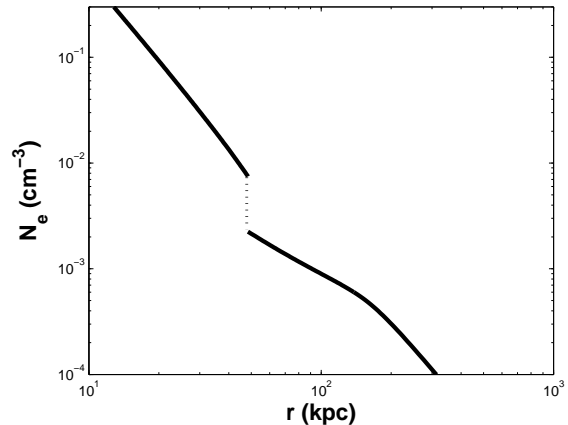


**Figure 4.** Electron number density profile for  $t = 7.59 \times 10^{15}$  s and  $K_2 = 5.50 \times 10^{20}$  SI unit on the downstream side of a shock for solution 2 (see Figs. 1 and 2 for details of the quasi-static solution behaviour at small  $x$ ). The corresponding global radial flow velocities of this solution are shown in Fig. 3. Here we take the typical mean molecular weight in clusters of galaxies to be 0.59 g/mol. As the electron number density can be obtained by high-resolution X-ray imaging observations, we give the model electron number density so that comparisons and tests can be made.

in Appendix G and the sound speed ratio in this specific example is displayed in Fig. 6.

According to expression (67), the temperature of hot ICM on the downstream side of the shock is  $\sim 0.85$  keV while the temperature on the upstream side is  $\sim 0.49$  keV. The enclosed mass of hot gas at 0.5Mpc is about  $M_2 = 2.4 \times 10^{12} M_\odot$ ; the enclosed mass ratio of dark matter halo to hot gas at 0.25Mpc is  $\sim 7.58$  and at 0.5Mpc is  $\sim 7.47$ . By expression (44), the outgoing shock speed in the hot

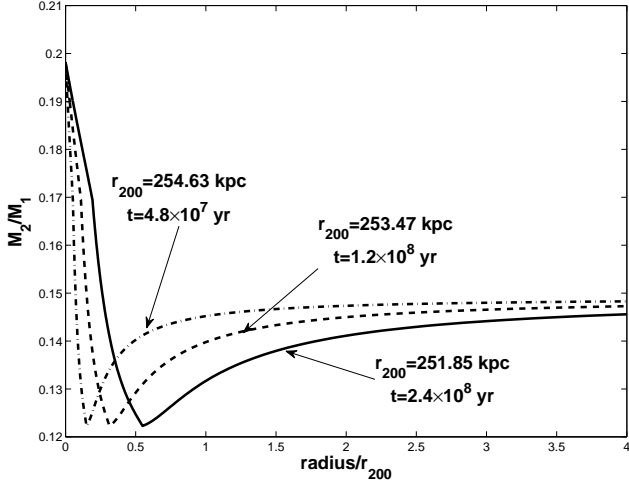


**Figure 5.** The enclosed mass ratio  $M_2/M_1$  as a function of  $r$  at different times of solution 2. The abscissa is the radius in the unit of virial radius  $r_{200}$  (defined in the paragraph before subsection 3.1) while the ordinate is the enclosed mass ratio  $M_2/M_1$  between the hot ICM and dark matter halo. The three curves are the enclosed mass ratio of solution 2 with the same parameter  $K_2 = 5.50 \times 10^{20}$  in SI unit on the downstream side of a shock but with different times as indicated along the curves. As for different times the virial radius  $r_{200}$  is a little different, the same position in the space corresponds to different radius in the figure in principle. However, the differences between the virial radius at different times are so small that we can treat one specific point of the  $x$  axis as the same position in the space at different times approximately.

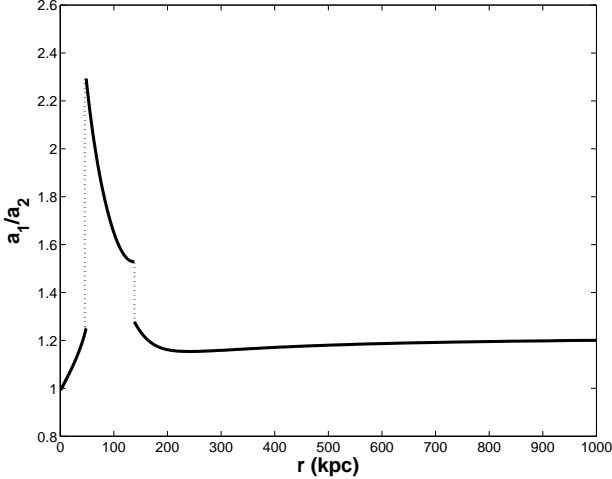


**Figure 6.** The radial profile for the polytropic sound speed ratio  $a_2/a_1$  of fluid 1 (dark matter) to fluid 2 (hot ICM) at time  $t = 7.59 \times 10^{15}$  for quasi-static solution 2 shown in Figs. 1 – 5. The first jump on the left at about  $r = 48.38$  kpc is due to the shock in fluid 2 (hot ICM) and the second jump on the right at about  $r = 138.23$  is due to the shock in fluid 1 (dark matter halo). When  $x \rightarrow 0^+$ , this ratio is about  $a_1/a_2 = 0.99$  and when  $x \rightarrow +\infty$  this ratio is about  $a_1/a_2 = 1.216$ .

ICM is  $u_{s,2} = nr_{s,2}/t = 157.6 \text{ km s}^{-1}$ . For a shock located at a radius of 48.38 kpc with a reference timescale of  $t = 2.4 \times 10^8 \text{ yr}$ , the shock position by equation (45) is  $r_{s,2} = 9.54 \times 10^{-6} t^{0.8}$  where  $r_{s,2}$  is in the unit of kpc and time  $t$  is in the unit of year. For example, during a timescale of  $\sim 10^{10} \text{ yr}$ , this shock would travel to a radius of  $\sim 1 \text{ Mpc}$  within a cluster of galaxies. The enclosed mass ratio  $M_2/M_1$  between the hot ICM and the dark matter of this solution at different radii is shown in Fig. 5 (the solid line with time  $t = 2.4 \times 10^8 \text{ yr}$ ). If we adjust the timescale, the solution will evolve in the self-similar manner. We choose two other timescales as examples with other parameters of solution 2 fixed and the result is also shown in Fig. 5. Note that with increasing time, the minimum of this ratio moves towards larger radii which is the result of accretion of hot gas and outflow of dark matter around the centre. The ratio remains nearly independent of time at the centre and at large radii.

As an example of conceptual exercise, we calculate at the reference time  $t_1 = 7.59 \times 10^{15} \text{ s}$  the energies within the radial range  $\sim 138 - 150.8$  kpc undisturbed by shocks. The gravitational potential energy is  $E_{grav,o} = -2.66 \times 10^{60} \text{ erg}$  by expression (70), the kinetic energy of fluid 1 is  $E_{k,1,o} = 4.94 \times 10^{57} \text{ erg}$  by expression (71), the kinetic energy of fluid 2 is  $E_{k,2,o} = 4.26 \times 10^{56} \text{ erg}$  by expression (71), the thermal energy of fluid 1 is  $E_{th,1,o} = 3.43 \times 10^{60} \text{ erg}$  by expression (72), and the thermal energy of fluid 2 is  $E_{th,2,o} = 2.72 \times 10^{59} \text{ erg}$  by expression (72). According to equation (75), the total energy is then  $E_{total,o} = 1.05 \times 10^{60} \text{ erg}$ . As  $r_{s,2} = 9.54 \times 10^{-6} t^{0.8}$ , the two shocks have passed through the radius 150.8 kpc by the time  $t_2 = 3.14 \times 10^{16} \text{ s}$ . Then at this time  $t_2$ , the energies within the same radial range are: the gravitational energy  $E_{grav,f} = -2.55 \times 10^{60} \text{ erg}$  by expression (70), the kinetic energy of fluid 1  $E_{k,1,f} = 1.0 \times 10^{56} \text{ erg}$  by expression (71), the kinetic energy of fluid 2  $E_{k,2,f} = 8.32 \times 10^{56} \text{ erg}$  by expression (71), the thermal energy of fluid 1  $E_{th,1,f} = 3.41 \times 10^{60} \text{ erg}$  by expression (72), and the thermal energy of fluid 2  $E_{th,2,f} = 3.09 \times 10^{59} \text{ erg}$  by expression (72). According to equation (75), the total energy is then  $E_{total,f} = 1.16 \times 10^{60} \text{ erg}$ . Then according to equation (76), the mean power of shock flow in this example is  $\mathcal{P}_{total} = 4.94 \times 10^{42} \text{ erg s}^{-1}$ .

Around a distance of  $r = 136$  kpc and with increasing  $r$ , the radial flow velocity of hot gas changes from inflow to outflow, where we can calculate the total mass accretion rate. We take a position  $r_a = 135.98$  kpc and the mass accretion rate there is then  $\dot{M}_{a,2} = 4\pi\rho_2 u_2 r_a^2 \approx 27.1 M_\odot \text{ yr}^{-1}$ , which is comparable to the mass accretion rates inferred for galaxy clusters A3158(P) and A262(P). There is a summary of these parameters for different clusters of galaxies, which are grossly consistent with our numerical example illustrated here (e.g., Peres et al 1998.)

At a radial distance of  $\sim 3 \text{ Mpc}$ , the outflow mass per year of hot ICM is  $\sim \dot{M}_{2,o} = 4\pi\rho_2 u_2 r^2 = 211 M_\odot \text{ yr}^{-1}$ . Thus the approximate total outflow mass of hot gas within a timescale of  $\sim 2.4 \times 10^8 \text{ yr}$  is  $5.1 \times 10^{10} M_\odot$ . Meanwhile, the inflow mass per year of dark matter is  $\sim \dot{M}_{1,o} = 4\pi\rho_1 u_1 r^2 = 140 M_\odot \text{ yr}^{-1}$ . Then the total inflow mass of dark matter within a timescale of  $2.4 \times 10^8 \text{ yr}$  is approximately  $\sim 3.36 \times 10^{10} M_\odot$ . Here, we take the timescale of galaxy cluster winds to be  $\sim 6 \times 10^9 \text{ yr}$ . Then during this time, we assume for simplicity that there is an AGN in a cluster of galaxies every  $2.4 \times 10^8 \text{ yr}$  and the

hot gas mass of  $\sim 5.1 \times 10^{10} M_\odot$  is lost and the dark matter mass of  $\sim 3.36 \times 10^{10} M_\odot$  is deposited each time. (That means there have been roughly 25 times of AGN activities in galaxy clusters since initial galaxy cluster winds formed.) Furthermore, when galaxy cluster winds began to form, we may presume that the baryon mass fraction  $f_b$  is roughly the average cosmic baryon fraction in the expanding universe. In this example, the total mass of hot ICM within 3 Mpc is  $6.1 \times 10^{12} M_\odot$  and the total mass of dark matter within this same radial scale is  $4.1 \times 10^{13} M_\odot$  at present. Then the value of baryon fraction  $f_b$  at present is 0.129 while the value of baryon fraction  $f_b$  when this cluster of galaxies begins to blow a galaxy cluster wind is 0.154. Therefore the baryon fraction  $f_b$  decreases 16.4% due to galaxy cluster winds and the inflow or contraction of dark matter halo in this example of illustration. In this scenario, the ‘missing baryons’ should be found in the periphery of galaxy clusters on much larger scales. They cool down to lower temperatures and may not be easily detected.

### 3.5 Solution Examples of $n = 1$

When  $n = 1$ , the radial flow velocities of both fluids approach constant values as  $x \rightarrow +\infty$ ; for global semi-complete solutions, these values can be negative, zero or positive at large  $x$ , depending on the choice of relevant parameters and positions of shocks. With  $n = 1$ , the asymptotic constant speeds are  $H_1$  and  $H_2$  in asymptotic velocity solutions (30) and (31) respectively. Physically, these correspond to inflows, breezes or contractions, and outflows, respectively. As  $x \rightarrow 0^+$ , flow solutions can be matched with the asymptotic quasi-static solution for both fluids. For  $n = 1$ , the mass density profile is  $\rho_i \rightarrow r^{-2}$  either as  $r \rightarrow 0^+$  or as  $r \rightarrow +\infty$ . We now provide a few examples with parameters  $\{n, \gamma_1, \gamma_2, \kappa\} = \{1, 1.3, 1.405, 4\}$  and corresponding values of  $\{A_1, A_2, k\}$  being  $\{267.2, 38.4, 1.89\}$ . Similar to the case of  $2/3 < n < 1$  as described in the previous subsection, we start the numerical integration with a small enough  $x_{ini}$  and go to a large enough  $x_{max}$ . Once  $v_1(x)$  and  $v_2(x)$  become constant after numerical integrations in a certain small  $x$  range, we would regard the  $x_{max}$  as sufficiently large. The results are shown in Fig. 7 to Fig. 10 and the relevant model parameters are summarized in Table 3. Specifically for these solutions 5, 6 and 7, the nine parameters to determine a dimensionless solution are:  $\{n, \gamma_1, \gamma_2, \kappa, L_1, L_2, x_{ini}, x_{d,1}, x_{d,2}\} = \{1, 1.3, 1.405, 4, 2.66 \times 10^{-3}, -0.0913, 1 \times 10^{-8}, 25.1, 6.5\}$  for solution 5;  $\{n, \gamma_1, \gamma_2, \kappa, L_1, L_2, x_{ini}, x_{d,1}, x_{d,2}\} = \{1, 1.3, 1.405, 4, 9.67 \times 10^{-4}, -0.0331, 3 \times 10^{-8}, 15, 9.5\}$  for solution 6; and  $\{n, \gamma_1, \gamma_2, \kappa, L_1, L_2, x_{ini}, x_{d,1}, x_{d,2}\} = \{1, 1.3, 1.405, 4, 9.67 \times 10^{-4}, -0.0331, 3 \times 10^{-8}, 12, 9.5\}$  for solution 7.

Again, we use solution 6 to further illustrate the process of a galaxy cluster wind. Here, fluid 1 represents the dark matter halo and fluid 2 represents the hot ICM. We choose the parameters  $t$  and  $K_2$  (the value on the downstream side of an ICM shock) as  $t = 6.32 \times 10^{15}$  s and  $K_2 = 7.34 \times 10^8$  SI unit. In this example, the shock positions in the hot ICM and in dark matter halo are  $r_{s,2} = 210.75$  kpc and 332.76 kpc, respectively. In galaxy cluster Hydra A, the observed shock is located at  $\sim 211$  kpc (e.g., Nulsen et al. 2005b) and the shock in galaxy cluster Ms0735.6+7421 is at  $\sim 240$  kpc (e.g., McNamara et al. 2005). For this example, we ap-

**Table 3.** Model parameters for solutions in Fig. 7 to Fig. 10 with  $n = 1$ . Here, No. on the left gives the numeric label to distinguish different solutions. Type 1 is the type of solutions for fluid 1 (dark matter halo) when  $x \rightarrow +\infty$  and Type 2 is the type of solutions for fluid 2 (hot ICM) when  $x \rightarrow +\infty$ . Here,  $x_{d,1}$  and  $x_{d,2}$  are the independent self-similar variables on the downstream sides of the respective shock positions for fluids 1 and 2.  $E_1$  is the coefficient of  $\alpha_1$  and  $E_2$  is the coefficient of  $\alpha_2$  at a sufficiently large  $x$  (see asymptotic solution 28 and 29).  $H_1$  is the velocity of fluid 1 at a sufficiently large  $x$  and  $H_2$  is the velocity of fluid 2 at a sufficiently large  $x$  (see equations 30 and 31). As this table is too long horizontally, we break this table into two parts and stack them together.

No.	Type 1	Type 2	$L_1$	$L_2$	$x_{ini}$
5	outflow	outflow	$2.66 \times 10^{-3}$	-0.0913	$1 \times 10^{-8}$
6	inflow	outflow	$9.67 \times 10^{-4}$	-0.0331	$3 \times 10^{-8}$
7	inflow	inflow	$9.67 \times 10^{-4}$	-0.0331	$3 \times 10^{-8}$
$x_{d,1}$	$x_{d,2}$	$E_1$	$E_2$	$H_1$	$H_2$
25.1	6.5	487	33.3	7.84	49.5
15	9.5	265	30.5	-0.811	10.34
12	9.5	200	28.2	-5.00	-2.34

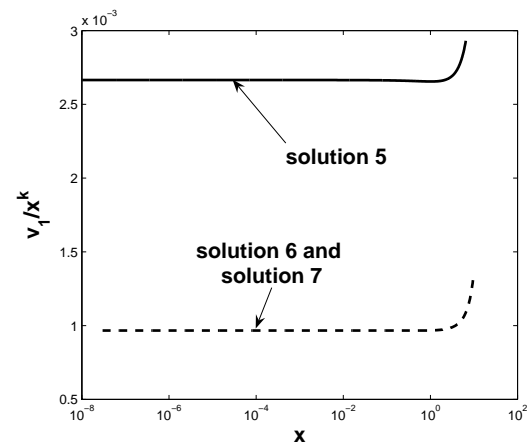


**Figure 7.** Scaled radial flow velocities of fluid 1 (dark matter) at small  $x$  when  $n = 1$ . The relevant model parameters are summarized in Table 3. Note that for a certain range of radial distance around small  $x$ ,  $v_1/x^k$  remains constant, showing that these solutions 5, 6 and 7 for  $v_1$  are indeed quasi-static solutions as derived analytically. For all these three solutions 5, 6 and 7, we have the same parameter set  $\{n, \gamma_1, \gamma_2, \kappa\} = \{1, 1.3, 1.405, 4\}$ . The corresponding flow velocities of fluid 2 (hot ICM) are shown in Fig. 8.

ply our model to the radial domain of  $\sim 1$  Mpc (some rich clusters of galaxies may have radial size scales of  $\sim 1 - 2$  Mpc; e.g., Bahcall 1996). The radial flow velocity profiles are shown in Fig. 11 while the profiles of electron number density and ICM temperature are displayed in Figs. 12 and 13, respectively. Actually the temperature profile similar to Fig 13 in the entire radial range has been observed in galaxy

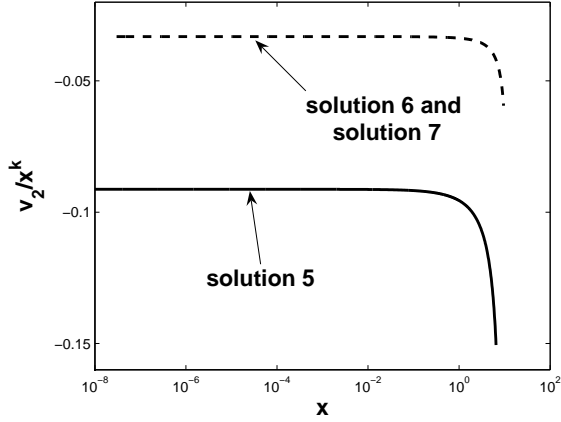


**Figure 8.** Radial flow velocities of fluid 2 (hot gas) at small  $x$  when  $n = 1$ . The relevant model parameters are listed in Table 3. Note that for a certain range of initial distance,  $v_2/x^k$  remains constant, which shows that these solutions of  $v_2$  are indeed quasi-static solutions. Together with Fig. 7 for radial flow velocities of fluid 1 (dark matter halo), we have succeeded in constructing solutions with both fluids being quasi-static at small  $x$ . For all these solutions, we have the same  $\{n, \gamma_1, \gamma_2, \kappa\} = \{1, 1.3, 1.405, 4\}$ .

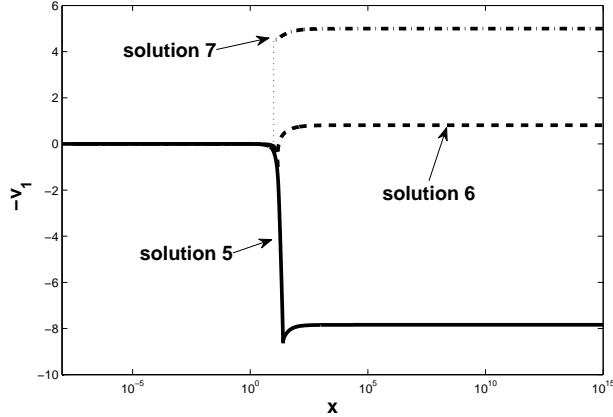


**Figure 9.** Radial flow velocities of fluid 1 (dark matter halo) at large  $x$  for  $n = 1$ . The relevant model parameters are listed in Table 3 with  $\{n, \gamma_1, \gamma_2, \kappa\} = \{1, 1.3, 1.405, 4\}$ . As shown in this figure,  $v_1$  remains constant for these three solutions at large  $x$ , indicating that the  $x_{max}$  we adopt is large enough for the asymptotic behaviour of  $v_1(x)$ . The radial flow velocities of fluid 1 at small  $x$  for these three solutions are shown in Fig. 7. The shock of solution 5 locates at the turning point  $x = 25.1$ , jumping from  $v_1 = 8.645$  to  $v_1 = 8.589$  and the shock of solution 6 locates at  $x = 15$ , jumping from  $v_1 = 0.99$  to  $v_1 = 0.3$ .

cluster NGC1275 (e.g., Churazov et al. 2003). The ratio of polytropic sound speeds (see Appendix G) in two fluids in this example is shown in Fig. 15. In this example, the radial outflow velocity of hot ICM at 1Mpc is  $\sim 97.4 \text{ km s}^{-1}$  and the radial inflow velocity of dark matter halo at 3 Mpc is  $\sim 66.76 \text{ km s}^{-1}$ . The temperature of hot ICM downstream of the shock is  $\sim 9.56 \text{ keV}$  and that of the upstream of the shock is  $\sim 7.9 \text{ keV}$ . The enclosed mass of hot ICM at 0.5Mpc is about  $M_2 = 4 \times 10^{13} M_\odot$ ; and the enclosed mass ratio of dark matter halo to hot ICM at 0.25Mpc is  $\sim 8.1$

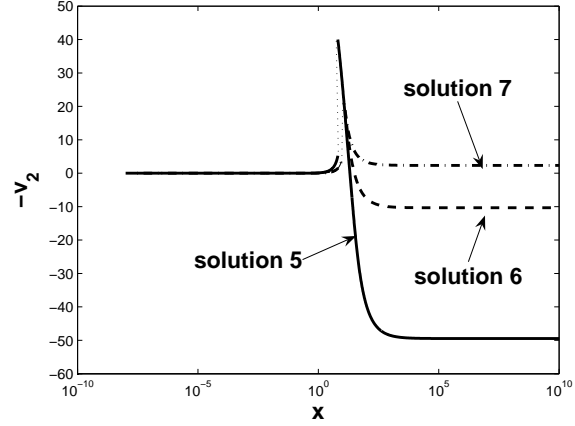


**Figure 10.** Radial flow velocities of fluid 2 at large  $x$  when  $n = 1$ . The relevant model parameters are listed in Table 3 with  $\{n, \gamma_1, \gamma_2, \kappa\} = \{1, 1.3, 1.405, 4\}$ . As shown in this figure,  $v_2$  remains constant for these three solutions at large  $x$ , indicating that the  $x_{max}$  we adopt is sufficiently large for the asymptotic behaviour of  $v_2(x)$ . For solutions 6 and 7, the shock positions are the same in gas but are different in dark matter halo (see Fig. 9). Together with Fig. 9, we have succeeded in constructing the semi-complete solutions with  $n = 1$ . The radial flow velocities of fluid 2 at small  $x$  for these solutions are shown in Fig. 8.

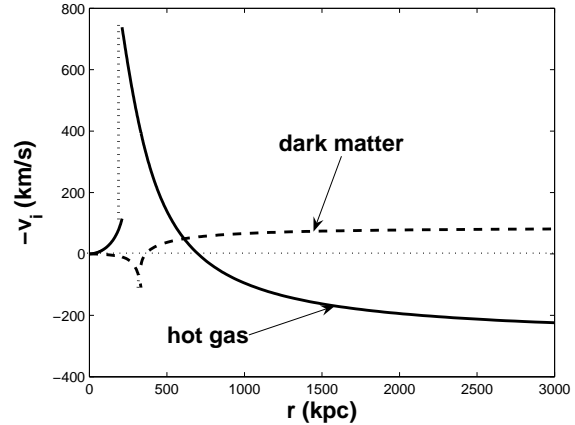


**Figure 11.** Radial flow velocities of hot ICM (solid curve) and dark matter halo (dashed curve) of solution 6 with  $n = 1$ ,  $t = 6.32 \times 10^{15}$  and  $K_2 = 7.34 \times 10^8$  SI unit in the downstream side of a shock in hot ICM. The shock positions in hot ICM and dark matter halo are at  $\sim 210.75 \text{ kpc}$  and at  $\sim 332.76 \text{ kpc}$ . The initial parameters for numerical integration are listed in Table 3 (solution 6). Details of the dimensionless velocities of this solution are shown in Figs. 7, 8, 9, 10 (solution 6).

and at 0.5Mpc is  $\sim 9.3$ . The travel speed of the outgoing shock in the hot ICM is  $u_{s,2} = nr_{s,2}/t = 1.03 \times 10^3 \text{ km s}^{-1}$ . For a shock located at 210.75 kpc with a timescale of  $t = 2 \times 10^8 \text{ yr}$ , the shock position (see expression (45)) can be calculated by  $r_{s,2} = 1.05 \times 10^{-6} t$  where  $r_{s,2}$  is in the unit of kpc and time  $t$  is in the unit of year. For  $n = 1$ , the shock speed remains constant. The enclosed mass ratio  $M_2/M_1$  between the hot ICM and the dark matter of this solution 6 shown Figs. 7 – 13 at different radii is displayed in Fig. 14 (the solid line with time  $t = 2 \times 10^8 \text{ yr}$ ). If we



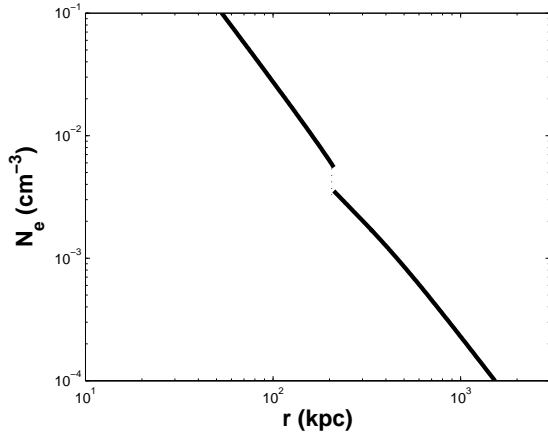


**Figure 12.** The radial profile of electron number density with a timescale of  $t = 6.32 \times 10^{15}$  s and  $K_2 = 7.34 \times 10^8$  SI unit on the downstream side of a shock in the hot ICM for solution 6 of  $n = 1$ . Here, we also take the typical mean molecular weight in clusters of galaxies to be  $\sim 0.59$  g/mol. The radial flow velocities of this solution 6 are shown in Fig. 11.

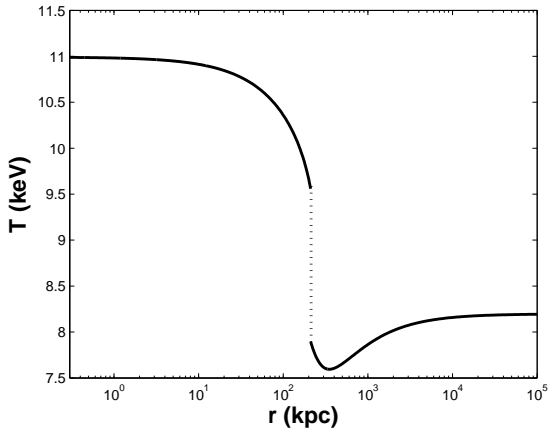


**Figure 13.** The radial temperature profile of hot ICM with a timescale of  $t = 6.32 \times 10^{15}$  s and  $K_2 = 7.34 \times 10^8$  SI unit on the downstream side of a shock in ICM for solution 6 of  $n = 1$ . During a range of short radial distance from the centre, the temperature is a constant of  $\sim 11$  keV and at large  $x$  the temperature is  $\sim 8.2$  keV. The electron number density of this solution 6 is shown in Fig. 12 and the corresponding radial flow velocities are shown in Fig. 11.

adjust the timescale  $t$ , solution 6 will evolve in a self-similar manner. We choose two other timescales  $t = 10^8$  yr (dashed curve) and  $4 \times 10^7$  yr (dash dotted curve) as two additional examples with other parameters of solution 6 unchanged and the results are shown in Fig. 14. With increasing time  $t$ , the minimum of this enclosed mass ratio moves towards larger radii which is the result of accretion of hot ICM and outflow of dark matter around the centre. This enclosed mass ratio is nearly independent of time  $t$  around the centre and at large radii.

As another example of conceptual exercise, we calculate at a reference time  $t = 6.32 \times 10^{15}$  s the energies within radial range  $\sim 332.7 - 502$  kpc undisturbed by shocks below. The

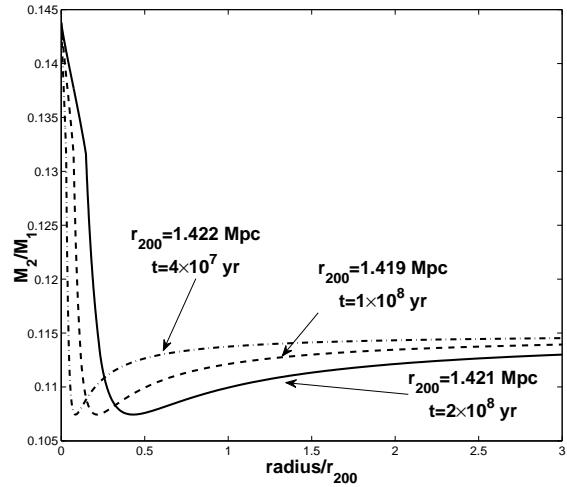


**Figure 14.** The radial profile of enclosed mass ratio  $M_2/M_1$  at different times of solution 6 shown in Figs. 7 – 13. The abscissa is the radius in unit of virial radius  $r_{200}$  and the ordinate is the enclosed mass ratio  $M_2/M_1$  between the hot ICM and dark matter. The three curves are enclosed mass ratio of solution 6 with the same parameter  $K_2 = 7.34 \times 10^8$  SI unit on the downstream side of an ICM shock and three different times  $t$  marked along the curves. As for different times the virial radius  $r_{200}$  is a somewhat different, the same position in space corresponds to different radii in this figure. However, these differences among the virial radii at different times are so small that we may treat one specific point of the abscissa as the same position in space at different times approximately.

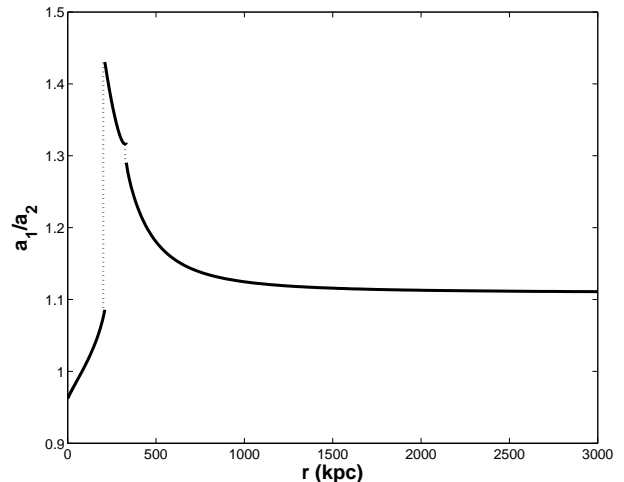


**Figure 15.** The radial profile for the ratio  $a_1/a_2$  of polytropic sound speeds in fluid 1 (dark matter) to fluid 2 (hot ICM) at time  $t = 6.32 \times 10^{15}$  for quasi-static solution 6 shown in Figs. 7 – 14. The first jump on the left at about  $r = 210.75$  kpc is due to the shock in fluid 2 and the second jump on the right at about 332.76 kpc is due to the shock in fluid 1. When  $x \rightarrow 0^+$ , this sound speed ratio is about  $a_1/a_2 = 0.962$  and when  $x \rightarrow +\infty$ , this ratio is about  $a_1/a_2 = 1.11$ .

gravitational energy is  $E_{grav,o} = -9.74 \times 10^{63}$  erg (see equation 70), the kinetic energy of fluid 1 is  $E_{k,1,o} = 7.39 \times 10^{59}$  erg (see equation 71), the kinetic energy of fluid 2 is  $E_{k,2,o} = 8.42 \times 10^{60}$  erg (see equation 71), the thermal energy of fluid 1 is  $E_{th,1,o} = 1.97 \times 10^{64}$  erg (see equation 72), the thermal energy of fluid 2 is  $E_{th,2,o} = 1.05 \times 10^{63}$  erg (see equation 72). According to equation (75), the total energy is then given by  $E_{total,o} = 1.11 \times 10^{64}$  erg. As  $r_{s,2} = 1.05 \times 10^{-6}t$ , the two shocks have passed through the radius 502 kpc by time  $t_2 = 1.50 \times 10^{16}$  s. Then at this time the energies within the same radial range are: the gravitational energy  $E_{grav,f} = -1.01 \times 10^{64}$  erg (see equation 70), the kinetic energy of fluid 1  $E_{k,1,f} = 5.78 \times 10^{58}$  erg (see equation 71), the kinetic energy of fluid 2  $E_{k,2,f} = 7.76 \times 10^{59}$  erg (see equation 71), the thermal energy of fluid 1  $E_{th,1,f} = 1.97 \times 10^{64}$  erg (see equation 72), the thermal energy of fluid 2  $E_{th,2,f} = 1.73 \times 10^{63}$  erg (equation 72). According to equation (75), the total energy is then  $E_{total,f} = 1.13 \times 10^{64}$  erg. Then according to equation (76), the mean power of shock flow in this illustration example is  $\mathcal{P}_{total} = 2.94 \times 10^{46}$  erg  $s^{-1}$ .

Around a radial distance of 695.5 kpc and with increasing  $r$ , the flow velocity of hot gas changes from inflow to outflow, where we can calculate the total mass accretion rate. We take a radius of  $r_a = 695$  kpc and the mass accretion rate is then  $\dot{M}_{a,2} = 4\pi\rho_2 u_2 r_a^2 \approx 193M_\odot \text{ yr}^{-1}$ , comparable to the mass accretion rates in galaxy clusters A85(P) and A644(P) (e.g., Peres et al. 1998).

At a radius of  $\sim 1\text{Mpc}$ , the outflow mass per year of hot ICM is  $\sim \dot{M}_{2,o} = 4\pi\rho_2 u_2 r^2 = 8.11 \times 10^3 M_\odot \text{ yr}^{-1}$ , which is comparable to the steady wind result of Yahil & Ostriker (1973). Thus the approximate total outflow mass of hot gas within a timescale of  $\sim 2 \times 10^8$  year is  $\sim 1.6 \times 10^{12} M_\odot$ . Meanwhile, the inflow mass per year of dark matter is  $\sim \dot{M}_{1,o} = 4\pi\rho_1 u_1 r^2 = 4.94 \times 10^4 M_\odot \text{ yr}^{-1}$ . Then the total inflow mass of dark matter within a timescale of  $2 \times 10^8$  yr is approximately  $10^{13} M_\odot$ . Here, we take the timescale of galaxy cluster winds to be  $3 \times 10^9$  yr and the AGN activity occurs every  $2 \times 10^8$  yr. (That means there have been roughly 15 times of AGN activities in galaxy clusters since the initial wind formed.) In this example, the total mass of hot ICM within 1 Mpc is  $8.1 \times 10^{13} M_\odot$  and the total mass of dark matter within this same radial scale is  $\sim 7.4 \times 10^{14} M_\odot$  at present. Now consider the mass loss of hot ICM due to galaxy cluster winds and inflow of dark matter. The total mass of hot ICM within this radial domain when the galaxy cluster winds began to form was  $1.05 \times 10^{14} M_\odot$  and the total mass of dark matter within this same radial domain when the galaxy cluster winds began to form was  $5.96 \times 10^{14} M_\odot$ . Therefore the baryon fraction  $f_b$  at present is 0.098 and its value when the cluster began to form winds is 0.15. The value of  $f_b$  decreases 34.7% due to galaxy cluster winds and inflow of dark matter halo in this example of  $n = 1$ .

### 3.6 Solution Examples of $n > 1$

With  $n > 1$  in our model, radial flow velocities of hot gas and dark matter will tend to diverge for  $H_1 \neq 0$  and  $H_2 \neq 0$  as we integrate towards  $x \rightarrow +\infty$  (see asymptotic solutions (30) and (31) towards large  $x$ ) with quasi-static asymptotic solutions around the cluster centre. This case of  $n > 1$  can be relevant as the density profile scales as  $\rho \propto r^{-2/n}$  while in many clusters of galaxies the electron number densities

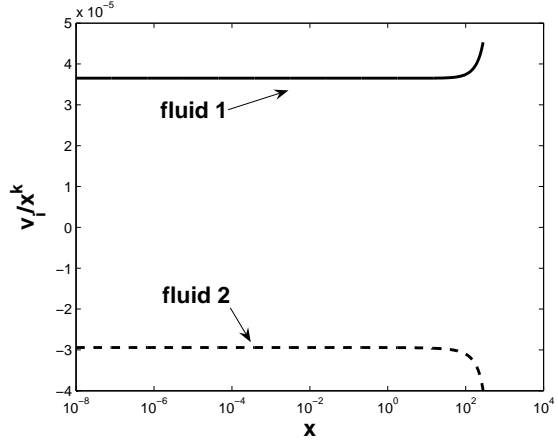


**Figure 16.** The scaled radial flow velocities as  $x \rightarrow 0^+$  for convergent solutions at large  $x$  when  $n > 1$  and with  $H_1 = H_2 = 0$ . The model parameters at small  $x$  are  $\{n, \gamma_1, \gamma_2, \kappa, x_{ini}, L_1, L_2\} = \{1.07, 1.315, 1.42, 0.1, 1 \times 10^{-8}, 3.65 \times 10^{-5}, -2.94 \times 10^{-5}\}$ . This figure shows that the solution approaches quasi-static configuration for both fluids with this set of parameters at small  $x$ . These parameters are kept the same as we try to find the convergent solution. So the solution we find here is still quasi-static at small  $x$ .

observed scale as a power law with power indices between  $-1$  and  $-2$  (e.g., clusters of galaxies A2204, A2052 and Ms0735.6+7421). So for a physical system, we only apply our model to a finite size of the order of  $\sim 1$  Mpc, which is the size of a typical cluster of galaxies. Therefore, we have considerable interest in those solutions with two coefficients  $H_1$  and  $H_2$  of the diverging terms being zero. We are now in a position to show such an example of solutions with  $n > 1$ .

In our model, we choose relevant parameters to be  $\{n, \gamma_1, \gamma_2, \kappa\} = \{1.07, 1.315, 1.42, 0.1\}$  with the corresponding values of  $\{A_1, A_2, k\} = \{1.53 \times 10^5, 2.27 \times 10^4, 1.81\}$ . The parameters at small  $x$  are  $\{x_{ini}, L_1, L_2\} = \{1 \times 10^{-8}, 3.65 \times 10^{-5}, -2.94 \times 10^{-5}\}$ . The radial flow velocities at small  $x$  are shown in Fig. 16, confirming that the solution we find is indeed quasi-static as  $x \rightarrow 0^+$ . By numerical exploration, we can choose proper values of independent self-similar variables  $x_{d,1}$  and  $x_{d,2}$  on the downstream sides of respective shock positions and construct a solution with  $H_1 = 0$  and  $H_2 = 0$  (i.e., finite radial flow velocities at large  $x$ ). With the relevant parameters chosen for small  $x$ , we vary the shock positions in fluid 1 and fluid 2, respectively, and compute the coefficients  $H_1$  and  $H_2$ . When the product  $v_i(x) x^{-1+1/n}$  approaches constant values for either values of  $i$  after a certain  $x_{max}$ , we would regard  $x$  as being large enough for asymptotic solutions and then evaluate the values of  $H_1$  and  $H_2$ . Empirically, we find that for a fixed  $x_{d,2}$  value, if we change the value of  $x_{d,1}$  continuously,  $H_1$  and  $H_2$  lie on a perfect straight line. When we vary  $x_{d,2}$ , this  $H_1$  versus  $H_2$  line will move. For a certain  $x_{d,2}$ , this line can move across the zero point in the functional relation of  $H_1$  versus  $H_2$ . When this happens, there exists a pair of  $\{x_{d,1}, x_{d,2}\}$  such that  $H_1 = H_2 = 0$ . This corresponds to convergent radial flow velocities for both fluids at large  $x$ . The result is then shown in Fig. 17 and the relevant parameters are summarized in Table 4.

**Table 4.** Model parameters for constructing a solution of  $n > 1$  with  $H_1 = 0$  and  $H_2 = 0$ . Here,  $x_{d,1}$  and  $x_{d,2}$  are the independent self-similar variables on the downstream sides of the shock positions for fluid 1 (dark matter) and fluid 2 (hot ICM), respectively.  $H_1$  is the coefficient of  $v_1(x)$  and  $H_2$  is the coefficient of  $v_2(x)$  when  $x$  becomes sufficiently large. Other model parameters at small  $x$  are  $\{n, \gamma_1, \gamma_2, \kappa, x_{ini}, L_1, L_2\} = \{1.07, 1.315, 1.42, 0.1, 1 \times 10^{-8}, 3.65 \times 10^{-5}, -2.94 \times 10^{-5}\}$ .

$x_{d,2}$	$x_{d,1}$	$H_1$	$H_2$
285	550	-6.056	-0.1668
285	555	-1.595	0.07426
285	557	0.2219	0.1721
285	560	2.989	0.3208
285	565	7.736	0.5748
<hr/>			
280	550	-8.039	-0.3993
280	555	-3.647	-0.1681
280	557	-1.862	-0.0744
280	559	-0.0598	0.0199
280	565	5.4775	0.309
<hr/>			
277	553	-6.613	-0.3972
277	555	-4.860	-0.3067
277	560	-0.411	-0.0774
277	563	2.314	0.0625
277	565	4.1578	0.1569
<hr/>			
275	553	-7.406	-0.4851
275	555	-5.663	-0.3961
275	560	-1.242	-0.171
275	563	1.462	-0.0338
275	565	3.290	0.0587

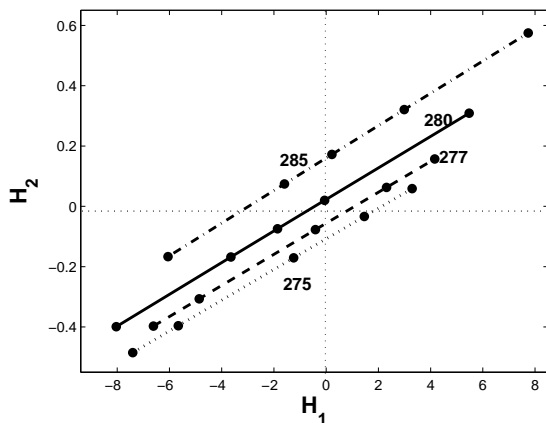


**Figure 17.** The numerical search of a global semi-complete solution of  $n > 1$  with  $H_1 = 0$  and  $H_2 = 0$ . As an example, the dash-dotted line marked by 285 is the line with  $x_{d,2} = 285$ . As  $x_{d,1}$  increases, the point goes from the bottom left to upper right (values of both  $H_1$  and  $H_2$  increase) along a straight line. Other straight lines are plotted in the same manner with different values of  $x_{d,2}$  as explicitly marked. The solid, heavy dashed, and dotted lines are with  $x_{d,2} = 280, 277, 275$ , respectively. The trend of variation is clear by this numerical exploration. The parameters of these four straight lines are summarized in Table 4. Other parameters at small  $x$  are  $\{n, \gamma_1, \gamma_2, \kappa, x_{ini}, L_1, L_2\} = \{1.07, 1.315, 1.42, 0.1, 1 \times 10^{-8}, 3.65 \times 10^{-5}, -2.94 \times 10^{-5}\}$ .

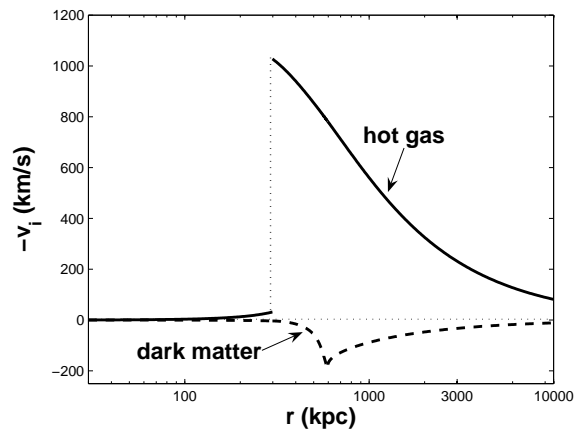


**Figure 18.** The radial flow velocities of hot ICM and dark matter halo of convergent solution with  $n > 1$ ,  $t = 1.1 \times 10^{16}$  s, and a downstream  $K_2 = 5.03 \times 10^6$  SI unit in the hot ICM. The shock position in hot ICM is at  $\sim 298.6$  kpc and the shock position in the dark matter halo is at  $\sim 596.2$  kpc. The relevant parameters for the numerical integration are  $\{n, \gamma_1, \gamma_2, \kappa, x_{ini}, L_1, L_2\} = \{1.07, 1.315, 1.42, 0.1, 1 \times 10^{-8}, 3.65 \times 10^{-5}, -2.94 \times 10^{-5}\}$ .

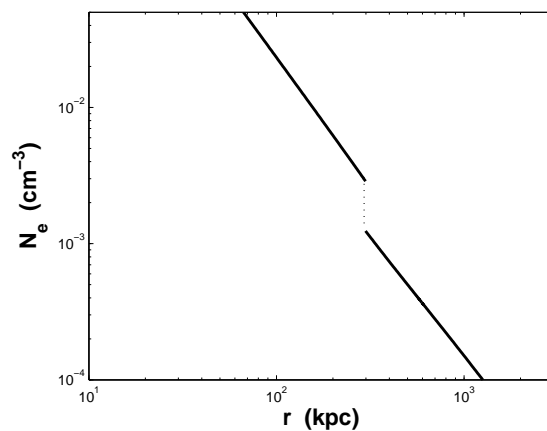


**Figure 19.** The electron number density profile of a convergent solution of  $n > 1$  with  $t = 1.1 \times 10^{16}$  s and  $K_2 = 5.03 \times 10^6$  in SI unit in the downstream side of the shock in the hot ICM. Here, we also take the typical mean molecular weight in galaxy clusters to be  $0.59$  g/mol (e.g., Cavaliere & Fusco-Femiano 1978). The other parameters are  $\{n, \gamma_1, \gamma_2, \kappa, x_{ini}, L_1, L_2\} = \{1.07, 1.315, 1.42, 0.1, 1 \times 10^{-8}, 3.65 \times 10^{-5}, -2.94 \times 10^{-5}\}$ .

From Fig. 17, we know the existence of a solution with convergent flow velocities at large  $x$  with  $x_{d,2} = 280$  and  $x_{d,1} = 559$ . We shall describe the physical process that this solution represents presently. The time  $t$  is chosen to be  $t = 1.1 \times 10^{16}$  s and the downstream  $K_2$  of hot ICM is chosen to be  $K_2 = 5.03 \times 10^6$  SI unit. Then the shock position in hot ICM is at  $\sim 298.6$  kpc and the shock in the dark matter halo is at  $\sim 596.2$  kpc.

We apply this numerical example to within a radial scale of  $\sim 3$  Mpc. The radial flow velocity profiles are shown in Fig. 18. If the two coefficients  $H_1$  and  $H_2$  are exactly zero, the hot gas velocity is inward and vanishes, while the flow velocity of dark matter is outward and vanishes as  $r \rightarrow$

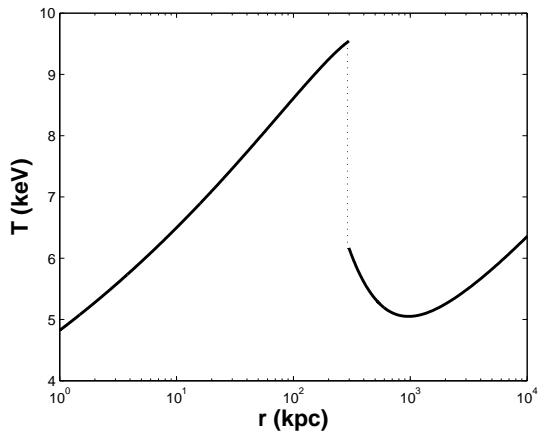


**Figure 20.** The temperature profile of hot ICM for a convergent solution at large  $x$  of  $n > 1$  with  $t = 1.1 \times 10^{16}$  s and  $K_2 = 5.03 \times 10^6$  in SI unit in the downstream side of the shock in the hot ICM. The temperature increases with increasing radius at both small and large  $x$ .

$+\infty$ . The profile of electron number density is shown in Fig. 19 and the temperature profile is shown in Fig. 20. In this example, the inflow velocity of hot gas at 3Mpc is about  $231.4 \text{ km s}^{-1}$  while the outflow velocity of dark matter at 3Mpc is  $\sim 32.8 \text{ km s}^{-1}$ . Across the shock, the temperature of hot ICM on the downstream side is  $\sim 9.5 \text{ keV}$  and that on the upstream side is  $\sim 6.17 \text{ keV}$ . The enclosed mass of hot ICM at 0.5Mpc is about  $M_2 = 3.33 \times 10^{13} M_\odot$ ; and the enclosed mass ratio of dark matter to the hot ICM at 0.25Mpc is  $\sim 7$  and at 0.5Mpc is  $\sim 9.5$ . The outgoing shock speed in the hot ICM is  $u_{s,2} = nr_{s,2}/t = 892 \text{ km s}^{-1}$ . For a shock located at  $r = 298.6 \text{ kpc}$  with a timescale of  $t = 3.8 \times 10^8 \text{ yr}$ , the shock position given by expression (45) can be followed by  $r_{s,2} = 2.2 \times 10^{-7} t^{1.07}$  where  $r_{s,2}$  is in the unit of kpc and time  $t$  is in the unit of year.

#### 4 SUMMARY

In this paper, we formulate a two-fluid model framework of spherical symmetry to explore dynamic behaviours of hot ICM and dark matter during the evolution of galaxy clusters. In this scenario, the hot ICM and dark matter halo are approximated as two polytropic ‘fluids’ and are coupled by gravity. For both ‘fluids’ in general situations, specific entropies are conserved along streamlines separately and are related to the enclosed masses. Quasi-static solutions for both ‘polytropic fluids’ can be obtained and are adopted for sufficiently small radii around the central core region at a given time. In order to construct dimensionless quasi-static solutions in the regime of small  $x$ , we need to specify nine dimensionless parameters  $\{n, \gamma_1, \gamma_2, \kappa, L_1, L_2, x_{ini}, x_{d,1}, x_{d,2}\}$  where  $x_{ini}$  needs to be properly chosen. Two additional dimensional parameters  $K_2$  and  $t$  need to be specified for dimensional solutions for a physical description. The ICM temperature is taken to be on the order of  $\sim 10^7 - 10^8 \text{ K}$  in typical clusters of galaxies and the electron number density is taken to be  $\sim 10^{-2} - 10^{-4} \text{ cm}^{-3}$  in the typical radial range of kpc to Mpc. It is possible to construct different types of flow solutions with shocks

in both fluids and with various asymptotic scaling features in flow speeds, mass densities, enclosed mass and temperatures. In particular, we can construct dynamic solutions for galaxy cluster winds and discuss the important problem of ‘missing baryons’ during the evolution of galaxy clusters. There are several physical hypotheses in our two-fluid model to simplify the mathematical analysis. First, we take the dark matter halo as a kind of ‘fluid’ for simplicity and explore this alternative theoretical possibility. Secondly, we assume the two-fluid system of galaxy clusters to be grossly spherically symmetric with a common centre and hope to catch major dynamic flow features on large scales. Thirdly, both ‘fluids’ are assumed to be ‘polytropic’ in the most general sense of entropy conservation along streamlines. In other words, the specific entropy distribution is not necessarily constant in space and time but are allowed to vary in  $r$  and  $t$  in general. Finally, dark matter interacts with the hot ICM only through gravity.

Global semi-complete solutions can be constructed to pass through the two singular surfaces via shocks in both fluids. As large-scale ICM shocks have been identified observationally, there must be large-scale flows of hot ICM. As the dark matter halo and the hot ICM are coupled by gravity, there may be dark matter flows and the possibility of shocks in dark matter halo. Such dark matter shocks are characterized by drastic density jumps and sharp rises of velocity dispersions and may be detected by utilizing gravitational lensing effects. In our model framework, outflows of hot ICM in galaxy clusters actually form galaxy cluster winds, which is a systematic mechanism of reducing the baryon fraction  $f_b$ . In our model, the self-similar shocks travel outwards in both hot ICM and dark matter halo, respectively. The travel speeds of these shocks actually change with time for  $n \neq 1$  and their radial positions at present can vary from tens of kpc to a few Mpc. Due to galaxy cluster winds, the baryon fraction  $f_b$  in galaxy clusters can be  $\sim 15\% - 40\%$  lower than the average cosmic baryon fraction in the Universe, which may account for the problem of ‘missing baryons’ in clusters of galaxies. Physically, these ‘missing baryons’ should reside in the periphery of galaxy clusters in the form of warm gas as results of unavoidable radiative cooling. Since the lower baryon fraction  $f_b$  is a generic phenomenon in clusters of galaxies, we therefore suggest that galaxy cluster winds would be common and frequent during the evolution of galaxy clusters.

The main features of our self-similar polytropic solution for two fluids coupled by gravity are summarized below. The radial profile of mass density at a given time is  $\rho_i \propto r^{-2/n}$  in both fluids for either  $r \rightarrow 0^+$  or  $r \rightarrow +\infty$  with  $2/3 < n < 2$  in general. That shows that the asymptotic mass density profiles of hot ICM and dark matter take the same form of power laws with the same index  $-2/n$ . Meanwhile, the radial flow velocities of both fluids approach zero as  $x \rightarrow 0^+$  in the form of quasi-static asymptotic solution (24) and (25). At large  $x$ , the asymptotic flow solution is (28), (29), (30), (31) for  $2/3 < n < 2$ . When  $2/3 < n < 1$  and  $x \rightarrow +\infty$ , the asymptotic radial flow velocities of both fluids approach zero. When  $n = 1$  and  $x \rightarrow +\infty$ , the radial flow velocities of both fluids approach constant values, which may be positive, zero or negative for various combinations of two fluids. When  $n > 1$  and  $x \rightarrow +\infty$ , the radial flow velocities of both fluids become divergent for  $H_1 \neq 0$  and  $H_2 \neq 0$  in asymptotic

solution (30) and (31). For  $H_1 = H_2 = 0$ , the radial flow velocities of both fluids remain finite at large  $x$  for  $n > 1$ . The radial profile of temperature in the hot ICM is  $T_2 \propto r^{2-2/n}$  for either  $r \rightarrow 0^+$  or  $r \rightarrow +\infty$ . By mass conservation, the enclosed mass is continuous across shocks.

## 5 DISCUSSION

There are several relevant aspects that may be further taken into account in our theoretical model development. First, we have ignored the magnetic field permeated in the hot ICM which has been observationally inferred to range from a few  $\mu\text{G}$  to several tens of  $\mu\text{G}$  in the central region (e.g., Fabian 1994; Carilli & Taylor 2002; Hu & Lou 2004). Cluster magnetic field can affect the gas dynamics in a nontrivial manner and can provide valuable diagnostic information such as synchrotron emission and modified Sunyaev-Zel'dovich effect (e.g., Hu & Lou 2004; Bagchi et al. 2006). To better understand behaviours of a magnetized hot gas and dark matter coupled by gravity, a magnetohydrodynamic (MHD) approach may be adopted (e.g., Lou & Wang 2007; Wang & Lou 2007). Secondly, we have assumed the flow system to be spherically symmetric, which is a highly idealized situation. Various instabilities may arise in dynamic flows to destroy spherical symmetry (Lou & Bai, 2007 in preparation). For systems of merging galaxies or galaxy clusters, spherical symmetry is only a gross approximation. Thirdly, our current model requires that the mass density profile has the same form of power law scalings either at small or large radii. If the scaling parameter  $n$  can be adjusted in some proper way across a shock, this model may be adapted to simulate more diverse kinds of galaxy clusters. Finally, it is possible to take a distribution function approach for dark matter halo and fluid description for the hot ICM to model a galaxy cluster as a further development. Admittedly, this approach could be mathematically challenging.

Compared with previous results, we note a few points regarding our model. First, our dynamic model of galaxy cluster wind differs from that of Yahil & Ostriker (1973). They considered a steady-state wind while the galaxy cluster wind of our model is dynamic and self-similar. Their gravitational potential is static and they did not model shock features occurred in galaxy clusters. Secondly, the case of  $n = 1$  for a single fluid sphere was discussed in Suto & Silk (1988). In addition to the major difference of two fluids coupled by gravity, our model with  $n = 1$  differs from that of Suto & Silk (1988) in that we have specific entropy conservation along streamlines. In Lou (2005), the model of two isothermal fluids coupled by gravity is discussed. Here, we treat two polytropic fluids coupled by self-gravity in more general situations. In particular, the quasi-static solution does not exist in an isothermal fluid (Lou & Wang 2006). By choosing different values of parameters  $n$ ,  $\gamma_i$ , and  $\kappa$  and shock positions, our polytropic model can be adapted to various astrophysical systems, including clusters of galaxies and globular clusters on much smaller scales.

Due to possible galaxy cluster winds, baryons in galaxy clusters can flow out of galaxy clusters and stay in their periphery. Meanwhile, dark matter halo contracts under gravity. As time goes on, such baryon gas cools down and may not be detectable in X-ray bands. This may naturally ex-

plain the problem of ‘missing baryons’ for clusters of galaxies. With this scenario in mind, we should develop observational diagnostics to look for signatures of these missing baryons around clusters of galaxies on much larger spatial scales ( $\gtrsim$  Mpc). In our perspective, the giant radio arcs recently discovered at 1.4GHz in galaxy cluster Abell 3376 (Bagchi et al. 2006) and the strikingly similar radio arcs in galaxy cluster 3667 (e.g., Rottgering et al. 1997; Roettiger et al. 1999) are most likely large-scale magnetohydrodynamic (MHD) shocks and imply large-scale flows around clusters of galaxies (Lou & Jiang 2008 in preparation).

As mentioned earlier, AGN activities are directly observed through intense electromagnetic radiation from normal matter. For AGN activities in the central region of a galaxy cluster, accretion of dark matter onto a SMBH may be involved (e.g., Hu et al. 2006) although dark matter activities cannot be directly detected. In this scenario, both ICM and dark matter coupled by gravity are active components of AGN activities and violent relaxation occurs in highly disturbed dark matter halo (Lynden-Bell 1967). In this sense, a dark matter halo gains gravitational energy and ‘thermal’ energy with higher velocity dispersions. Furthermore, shocks can also form in association with cluster merging processes also observed to occur in clusters of galaxies (e.g., the galaxy cluster 1E 0657-56; Clowe et al. 2006). In such merging processes, dark matter is dragged along and the energy may be transferred to the dark matter. This mechanism has already been discussed by some authors (e.g., Shchekinov & Vasiliev 2006; Knebe et al. 2002).

Very recently, caustics in dark matter halo have been discussed by many authors (e.g., Natarajan & Sikivie 2007; Onemli & Sikivie 2007; Mohayaee et al. 2007). Caustics are consequence of collisionless cold dark matter in galactic halos or clusters of galaxies. Caustics are regions of infinite density in the limit that the DM particles have zero velocity dispersion (e.g., Natarajan & Sikivie 2007). Gravitational lensing effects have been proposed to detect the existence of such caustics (e.g., Onemli & Sikivie 2007). Compared with sharp drops of DM density in caustics, shocks in dark matter halo of our model are different in that the discontinuity of DM density across shocks is less drastic. In general, the density on the downstream side of shocks are  $\sim 2 - 10$  times of the density on the upstream side of shocks. However, DM shocks share certain common features with DM caustics. They are both discontinuous surfaces in dark matter halo and both may be detected through gravitational lensing effects at least in principle.

## ACKNOWLEDGEMENT

This research was supported in part by Tsinghua Centre for Astrophysics (THCA), by National Natural Science Foundation of China (NSFC) grants 10373009 and 10533020 and National Basic Science Talent Training Foundation (NSFC J0630317) at Tsinghua University, and by the Yangtze Endowment and the SRFDP 20050003088 at Tsinghua University. Y.-F. Jiang and C.-C. Jin thank W.-G. Wang and F.-Y. Bian for useful discussion.

### APPENDIX A: SELF-SIMILAR NONLINEAR ORDINARY DIFFERENTIAL EQUATIONS

On the basis of reduced self-similar equations (13) – (16) in the section of Model Formulation, the reduced radial flow speeds  $v_1(x)$  and  $v_2(x)$  and the reduced mass densities  $\alpha_1(x)$  and  $\alpha_2(x)$  are determined by four coupled first-order nonlinear ODEs shown below.

$$d\alpha_1(x)/dx = \mathcal{A}_1(x)/\mathcal{D}_1(x), \quad (\text{A1})$$

$$dv_1(x)/dx = \mathcal{V}_1(x)/\mathcal{D}_1(x), \quad (\text{A2})$$

$$d\alpha_2(x)/dx = \mathcal{A}_2(x)/\mathcal{D}_2(x), \quad (\text{A3})$$

$$dv_2(x)/dx = \mathcal{V}_2(x)/\mathcal{D}_2(x). \quad (\text{A4})$$

The explicit expressions of the two denominators  $\mathcal{D}_1(x)$  and  $\mathcal{D}_2(x)$  are given by

$$\mathcal{D}_1(x) \equiv (nx - v_1)^2 - \gamma_1 \alpha_1^{q_1 + \gamma_1 - 1} x^{2q_1} (nx - v_1)^{q_1}, \quad (\text{A5})$$

and

$$\mathcal{D}_2(x) \equiv (\kappa nx - v_2)^2 / \kappa - \kappa^{2q_2 - 1} \gamma_2 \alpha_2^{q_2 + \gamma_2 - 1} x^{2q_2} (\kappa nx - v_2)^{q_2}. \quad (\text{A6})$$

The explicit expressions for the four numerators  $\mathcal{A}_1(x)$ ,  $\mathcal{V}_1(x)$ ,  $\mathcal{A}_2(x)$  and  $\mathcal{V}_2(x)$  are given by

$$\begin{aligned} \mathcal{A}_1(x) \equiv & \alpha_1 \left\{ q_1 \alpha_1^{q_1 + \gamma_1 - 1} x^{2q_1} (nx - v_1)^{q_1 - 1} (3n - 2) \right. \\ & + \frac{\alpha_1}{(3n - 2)} (nx - v_1) + \frac{\alpha_2}{(3n - 2)} \left( nx - \frac{v_2}{\kappa} \right) \\ & \left. + (n - 1)v_1 - \frac{2(x - v_1)(nx - v_1)}{x} \right\}; \quad (\text{A7}) \end{aligned}$$

$$\begin{aligned} \mathcal{V}_1(x) \equiv & q_1 \alpha_1^{q_1 + \gamma_1 - 1} x^{2q_1} (nx - v_1)^{q_1} (3n - 2) \\ & - 2\gamma_1 \alpha_1^{q_1 + \gamma_1 - 1} x^{2q_1 - 1} (nx - v_1)^{q_1} (x - v_1) \\ & + \frac{\alpha_1 (nx - v_1)^2}{(3n - 2)} + \frac{\alpha_2 (nx - v_1)}{(3n - 2)} \left( nx - \frac{v_2}{\kappa} \right) \\ & + (n - 1)(nx - v_1)v_1; \quad (\text{A8}) \end{aligned}$$

$$\begin{aligned} \mathcal{A}_2(x) \equiv & \alpha_2 \left\{ q_2 \kappa^{2q_2} \alpha_2^{q_2 + \gamma_2 - 1} x^{2q_2} (\kappa nx - v_2)^{q_2 - 1} (3n - 2) \right. \\ & + \frac{\alpha_2 (\kappa nx - v_2)}{(3n - 2)} + \frac{\kappa \alpha_1 (nx - v_1)}{(3n - 2)} \\ & \left. + (n - 1)v_2 - \frac{2(\kappa x - v_2)(\kappa nx - v_2)}{\kappa x} \right\}; \quad (\text{A9}) \end{aligned}$$

$$\begin{aligned} \mathcal{V}_2(x) \equiv & q_2 \kappa^{2q_2} \alpha_2^{q_2 + \gamma_2 - 1} x^{2q_2} (\kappa nx - v_2)^{q_2} (3n - 2) \\ & - 2\kappa^{2q_2 - 1} \gamma_2 \alpha_2^{q_2 + \gamma_2 - 1} x^{2q_2 - 1} (\kappa nx - v_2)^{q_2} (\kappa x - v_2) \\ & + \frac{\alpha_2 (\kappa nx - v_2)^2}{(3n - 2)} + \frac{\kappa \alpha_1 (nx - v_1)}{(3n - 2)} (\kappa nx - v_2) \\ & + (n - 1)(\kappa nx - v_2)v_2. \quad (\text{A10}) \end{aligned}$$

Here, all relevant dimensionless parameters are defined in the main text. With proper asymptotic solutions at large and small  $x$  and shock conditions across the sonic critical curves, we can construct global semi-complete self-similar solutions with shocks to model large-scale dynamics in a galaxy cluster involving hot ICM and dark matter halo.

### APPENDIX B: THE QUARTIC EQUATION FOR INDEX PARAMETER $K$

In equation (26), the index  $k$  for the quasi-static solution of two gravity coupled fluids are determined by the following quartic equation

$$C_{k,1} k^4 + C_{k,2} k^3 + C_{k,3} k^2 + C_{k,4} k + C_{k,5} = 0, \quad (\text{B1})$$

where the five coefficients  $C_{k,1}$ ,  $C_{k,2}$ ,  $C_{k,3}$ ,  $C_{k,4}$ , and  $C_{k,5}$  are explicitly determined by the following expressions

$$C_{k,1} \equiv n^4 \gamma_1 \gamma_2 \left( 1 + \frac{A_1}{A_2} \right) \left( 1 + \frac{A_2}{A_1} \right), \quad (\text{B2})$$

$$C_{k,2} \equiv (6n - 8)n^3 \gamma_1 \gamma_2 \left( 1 + \frac{A_1}{A_2} \right) \left( 1 + \frac{A_2}{A_1} \right), \quad (\text{B3})$$

$$\begin{aligned} C_{k,3} \equiv & \left\{ -3n^4 \gamma_1 \gamma_2 + n^2 (4 - 2n)(q_2 + \gamma_2 - 1) \right. \\ & \times [(2 - 3n)\gamma_1 - (4 - 2n)(q_1 - 1)] \\ & + n^2 (4 - 2n)(q_1 + \gamma_1 - 1)[(2 - 3n)\gamma_2 \\ & - (4 - 2n)(q_2 - 1)] + (4 - 2n)^2 n^2 (q_1 - 1)(q_2 - 1) \\ & \left. + (4 - 2n)^2 n^2 (q_1 + \gamma_1 - 1)(q_2 + \gamma_2 - 1) \right\} \\ & \times \left( 1 + \frac{A_1}{A_2} \right) \left( 1 + \frac{A_2}{A_1} \right) \\ & + (3n - 2)(4 - 2n)n^2 \gamma_1 \left( 1 + \frac{A_2}{A_1} \right) \\ & + (3n - 2)(4 - 2n)n^2 \gamma_2 \left( 1 + \frac{A_1}{A_2} \right), \quad (\text{B4}) \end{aligned}$$

$$\begin{aligned} C_{k,4} \equiv & 2 \left\{ [\gamma_2 n + (2 - n)(q_2 - 1)] n^3 \gamma_1 \right. \\ & + [\gamma_1 n + (2 - n)(q_1 - 1)] n^3 \gamma_2 \\ & - 4[(2 - n)(q_1 - 1) + \gamma_1 n][\gamma_2 n + (2 - n)(q_2 - 1)] n^2 \\ & + 2n(q_2 + \gamma_2 - 1)(2 - n)[n\gamma_1 + (2 - n)^2 (q_1 - 1)] \\ & + 2n(q_1 + \gamma_1 - 1)(2 - n)[n\gamma_2 + (2 - n)^2 (q_2 - 1)] \\ & \left. + 8(2 - n)^2 (n - 1)n(q_2 + \gamma_2 - 1)(q_1 + \gamma_1 - 1) \right\} \\ & \times \left( 1 + \frac{A_1}{A_2} \right) \left( 1 + \frac{A_2}{A_1} \right) \\ & + 2(3n - 2)(3n - 4)(2 - n)n\gamma_1 \left( 1 + \frac{A_2}{A_1} \right) \\ & + 2(3n - 2)(3n - 4)(2 - n)n\gamma_2 \left( 1 + \frac{A_1}{A_2} \right), \quad (\text{B5}) \end{aligned}$$

$$\begin{aligned}
 C_{k,5} \equiv & 4(3n-2)(2-n)(n^2-6n+4)\gamma_1 \left(1 + \frac{A_2}{A_1}\right) \\
 & + 4(3n-2)(2-n)(n^2-6n+4)\gamma_2 \left(1 + \frac{A_1}{A_2}\right) \\
 & + 4[\gamma_1 n + (2-n)(q_1-1)][\gamma_2 n + (2-n)(q_2-1)] \\
 & \quad \times n^2 \left(1 + \frac{A_1}{A_2}\right) \left(1 + \frac{A_2}{A_1}\right) \\
 & + 8[\gamma_1 n + (2-n)(q_1-1)](2-n)(q_2 + \gamma_2 - 1) \\
 & \quad \times n(n-1) \left(1 + \frac{A_1}{A_2}\right) \left(1 + \frac{A_2}{A_1}\right) \\
 & + 8[\gamma_2 n + (2-n)(q_2-1)](2-n)(q_1 + \gamma_1 - 1) \\
 & \quad \times n(n-1) \left(1 + \frac{A_1}{A_2}\right) \left(1 + \frac{A_2}{A_1}\right) \\
 & + 16(n-1)^2(2-n)^2(q_2 + \gamma_2 - 1) \\
 & \quad \times (q_1 + \gamma_1 - 1) \left(1 + \frac{A_1}{A_2}\right) \left(1 + \frac{A_2}{A_1}\right) \\
 & - 4(3n-2)^2(2-n)^2(q_1-1) \left(1 + \frac{A_2}{A_1}\right) \\
 & - 4(3n-2)^2(2-n)^2(q_2-1) \left(1 + \frac{A_1}{A_2}\right), \quad (\text{B6})
 \end{aligned}$$

where the two coefficients  $A_1$  and  $A_2$  in the static SPS solution (17) are determined by equation (18). In short, once the four parameters  $(n, \gamma_1, \gamma_2, \kappa)$  are specified, we should be able to determine the static SPS solution (17) and the corresponding quasi-static solution (24)–(27).

### APPENDIX C: QUASI-STATIC SOLUTIONS WITH COMPLEX $K$

For a complex  $k$  root with  $k = k_1 + ik_2$  with  $k_1$  and  $k_2$  being the real and imaginary parts of  $k$  (note that the value of  $k$  is the same for both fluids coupled by gravity), the four parameters  $L_1, L_2, N_1$  and  $N_2$  (the coefficients for radial flow speeds and mass densities at small  $x$  of quasi-static solutions defined in equation (24) and (25)) all become complex with  $L_1 = L_{1,1} + iL_{1,2}$ ,  $L_2 = L_{2,1} + iL_{2,2}$ ,  $N_1 = N_{1,1} + iN_{1,2}$ , and  $N_2 = N_{2,1} + iN_{2,2}$ , where the real and imaginary parts are all explicitly written out. As the static SPS solution (17) is real, we only take the real part as the quasi-static solution, namely

$$\begin{aligned}
 v_i(x) &= \text{Re}(L_i x^k) = \text{Re}[L_i x^{k_1} \exp(ik_2 \ln x)] \\
 &= x^{k_1} [L_{i,1} \cos(k_2 \ln x) - L_{i,2} \sin(k_2 \ln x)], \quad (\text{C1})
 \end{aligned}$$

$$\begin{aligned}
 \alpha_i(x) &= \text{Re} \left( A_i x^{-2/n} + N_i x^{k-1-2/n} \right) \\
 &= \text{Re} \left[ A_i x^{-2/n} + x^{-2/n-1+k_1} N_i \exp(ik_2 \ln x) \right] \\
 &= A_i x^{-2/n} + x^{-2/n-1+k_1} \\
 & \quad \times [N_{i,1} \cos(k_2 \ln x) - N_{i,2} \sin(k_2 \ln x)], \quad (\text{C2})
 \end{aligned}$$

where

$$\begin{aligned}
 n^2[(k_1-1)^2 + k_2^2]N_{1,1} &= (k_1-1)[2(n-1) \\
 & + nk_1]L_{1,1}A_1 + (3n-2)k_2L_{1,2}A_1 + nk_2^2L_{1,1}A_1, \quad (\text{C3})
 \end{aligned}$$

$$\begin{aligned}
 N_{1,2} &= N_{1,1}(k_1-1)/k_2 + L_{1,2}A_1/n \\
 & - [2(n-1) + nk_1]L_{1,1}A_1/(k_2n^2), \quad (\text{C4})
 \end{aligned}$$

$$\begin{aligned}
 n^2[(k_1-1)^2 + k_2^2]\kappa N_{2,1} &= (k_1-1)[2(n-1) \\
 & + nk_1]L_{2,1}A_2 + (3n-2)k_2L_{2,2}A_2 + nk_2^2L_{2,1}A_2, \quad (\text{C5})
 \end{aligned}$$

$$\begin{aligned}
 N_{2,2} &= N_{2,1}(k_1-1)/k_2 + L_{2,2}A_2/(\kappa n) \\
 & - [2(n-1) + nk_1]L_{2,1}A_2/(\kappa k_2 n^2). \quad (\text{C6})
 \end{aligned}$$

As equation (26) is a quartic equation for  $k$  involving real coefficients, it has either real roots or pairs of complex conjugate roots. With free parameters  $L_{i,1}$  and  $L_{i,2}$ , we can always choose the imaginary part of a complex root<sup>6</sup>  $k$  to be  $k_2 > 0$ .

For this type of quasi-static solutions with complex  $k$ , there are asymptotic oscillations as  $x \rightarrow 0^+$  (see also Lou & Wang 2006 for such oscillatory solution behaviours in a single fluid).

### APPENDIX D: ASYMPTOTIC SERIES SOLUTIONS AT LARGE $X$

As stated in subsection 2.4, for a given value of  $n$ , the asymptotic series solution of equations (13)–(16) at large  $x$  is in the form of

$$\alpha_1(x) \rightarrow E_1 x^{-2/n} + I_1 x^{-3/n} + \dots, \quad (\text{D1})$$

$$\alpha_2(x) \rightarrow E_2 x^{-2/n} + I_2 x^{-3/n} + \dots, \quad (\text{D2})$$

$$v_1(x) \rightarrow H_1 x^{-1/n+1} + G_1 x^{-2/n+1} + \dots, \quad (\text{D3})$$

$$v_2(x) \rightarrow H_2 x^{-1/n+1} + G_2 x^{-2/n+1} + \dots. \quad (\text{D4})$$

The four coefficients  $I_1, I_2, G_1$  and  $G_2$  can be expressed in terms of  $E_1, E_2, H_1$  and  $H_2$  as

$$\begin{aligned}
 G_1 &= \frac{(1-n)}{n} H_1^2 + 2(2-n)E_1^{q_1+\gamma_1+1} n^{q_1-1} \\
 & - \frac{n}{(3n-2)} (E_1 + E_2), \quad (\text{D5})
 \end{aligned}$$

$$\begin{aligned}
 G_2 &= \frac{(1-n)}{n} \frac{H_2^2}{\kappa} + 2(2-n)\kappa^{3q_2-1} E_2^{q_2+\gamma_2+1} n^{q_2-1} \\
 & - \frac{\kappa n}{(3n-2)} (E_1 + E_2), \quad (\text{D6})
 \end{aligned}$$

$$I_1 = \frac{3(1-n)}{n} H_1 E_1, \quad (\text{D7})$$

$$I_2 = \frac{3(1-n)}{n} \frac{H_2 E_2}{\kappa}. \quad (\text{D8})$$

For solutions with  $n > 1$  and  $H_1 = H_2 = 0$ , the asymptotic series solutions finite at large  $x$  become

$$\alpha_1(x) \rightarrow E_1 x^{-2/n} + F_1 x^{-4/n+1} + \dots, \quad (\text{D9})$$

<sup>6</sup> Parameter  $k_2$  is the imaginary part of a complex  $k$  index. If  $k_2 < 0$ , for the  $k_2$  that appears in function  $\cos(x)$ , it does not matter to choose it to be  $-k_2$ . For  $k_2$  that appears in function  $\sin(x)$ , as long as  $L_{i,2}$  being a free parameter, we can always choose it to be  $-L_{i,2}$  and it follows that  $N_{i,2}$  becomes  $-N_{i,2}$ . In this manner, solution for  $-k_2$  remains the same as that for  $k_2$ . In conclusion, there is no loss of generality to choose  $k_2 > 0$  to represent all possible solutions with free parameters  $L_i$ .

$$\alpha_2(x) \rightarrow E_2 x^{-2/n} + F_2 x^{-4/n+1} + \dots, \quad (D10)$$

$$v_1(x) \rightarrow G_1 x^{-2/n+1} + D_1 x^{-4/n+2} + \dots, \quad (D11)$$

$$v_2(x) \rightarrow G_2 x^{-2/n+1} + D_2 x^{-4/n+2} + \dots. \quad (D12)$$

The six coefficients  $G_1$ ,  $G_2$ ,  $F_1$ ,  $F_2$ ,  $D_1$ , and  $D_2$  are determined by specified values of  $E_1$  and  $E_2$  below

$$G_1 = 2(2-n)E_1^{q_1+\gamma_1+1}n^{q_1-1} - \frac{n(E_1+E_2)}{(3n-2)}, \quad (D13)$$

$$G_2 = 2(2-n)\kappa^{3q_2-1}E_2^{q_2+\gamma_2+1}n^{q_2-1} - \frac{\kappa n(E_1+E_2)}{(3n-2)}, \quad (D14)$$

$$F_1 = (4-3n)(2-n)E_1^{q_1+\gamma_1}n^{q_1-2} + \frac{(3n-4)}{2(3n-2)}E_1(E_1+E_2), \quad (D15)$$

$$F_2 = \kappa^{3q_2-2}(4-3n)(2-n)E_2^{q_2+\gamma_2}n^{q_2-2} + \frac{(3n-4)}{2(3n-2)}E_2(E_1+E_2), \quad (D16)$$

$$D_1 = \frac{2}{(3-n)} \left[ (2-n)(q_1+\gamma_1-1)E_1^{q_1+\gamma_1-2}n^{q_1-1}F_1 - \frac{n(F_1+F_2)}{2(3n-2)} \right], \quad (D17)$$

$$D_2 = \frac{2}{(3-n)} \left[ (2-n)\kappa^{3q_2-1}(q_2+\gamma_2-1) \times E_2^{q_2+\gamma_2-2}n^{q_2-1}F_2 - \frac{\kappa n(F_1+F_2)}{2(3n-2)} \right]. \quad (D18)$$

## APPENDIX E: EIGENDIRECTIONS ACROSS THE SONIC CRITICAL CURVE

For a specified pair of  $(\alpha_2, v_2)$  at a given  $x$ , we now determine the eigendirections across the sonic critical curve of fluid 1. The first equation in nonlinear ODEs (Equation (13)) gives

$$\frac{d\alpha_1}{dx} = \left[ \alpha_1 \frac{dv_1}{dx} - 2 \frac{(x-v_1)}{x} \alpha_1 \right] / (nx-v_1). \quad (E1)$$

We take  $n > 2/3$  and thus  $nx-v > 0$  in this paper. From  $\mathcal{D}_1(x) = 0$ , we obtain

$$v_1 = nx - \left[ \gamma_1 x^{2q_1} \alpha_1^{q_1+\gamma_1-1} \right]^{1/(2-q_1)}. \quad (E2)$$

From  $\mathcal{A}_1(x) = 0$ , the value of  $\alpha_1$  on the sonic critical curve at  $x$  is determined by the following equation

$$\begin{aligned} & \left( \frac{\alpha_1}{3n-2} + n + 1 + \frac{2n-4}{\gamma_1} \right) (\gamma_1 \alpha_1^{q_1+\gamma_1-1} x^{2q_1})^{1/(2-q_1)} \\ & - 2 \left( \gamma_1 \alpha_1^{q_1+\gamma_1-1} \right)^{2/(2-q_1)} x^{(5q_1-2)/(2-q_1)} \\ & = - \frac{\alpha_2}{(3n-2)} \left( nx - \frac{v_2}{\kappa} \right) - n(n-1)x. \end{aligned} \quad (E3)$$

In general, fluid 2 is not on the sonic critical curve at this position  $x$ . Therefore,  $\alpha'_2$  is determined by equation (15) while  $v'_2$  is determined by equation (16). We now apply the

L'Hôpital rule to determine the eigenvalues of  $v'_1(x)$  from equation (14)

$$\frac{dv_1(x)}{dx} = \frac{\mathcal{V}'_1(x)}{\mathcal{D}'_1(x)}. \quad (E4)$$

This equation appears to be a quadratic algebraic equation in terms of  $v'_1(x)$ , namely

$$C_{v,1} [v'_1(x)]^2 + C_{v,2} v'_1(x) + C_{v,3} = 0, \quad (E5)$$

where the three coefficients  $C_{v,1}$ ,  $C_{v,2}$ ,  $C_{v,3}$  are explicitly defined by

$$C_{v,1} \equiv 1 + \alpha_1^{q_1+\gamma_1-1} \gamma_1^2 x^{2q_1} (nx-v_1)^{q_1-2}, \quad (E6)$$

$$C_{v,2} \equiv \alpha_1^{q_1+\gamma_1-1} \gamma_1 x^{2q_1-1} (nx-v_1)^{q_1-2} \{ 4(\gamma_1-1)v_1 + [3n(q_1+1) - 2(q_1+\gamma_1+1)]x \} - 1, \quad (E7)$$

$$\begin{aligned} C_{v,3} \equiv & 2\alpha_1^{q_1+\gamma_1-1} x^{2q_1-2} (nx-v_1)^{q_1-2} \left\{ \gamma_1(2\gamma_1-1)v_1^2 \right. \\ & + \left[ n(3q_1\gamma_1-2) - 2[\gamma_1(q_1+\gamma_1+1) - 2] \right] xv_1 \\ & \left. - (n-2)[n-3nq_1+2(q_1+\gamma_1-1)]x^2 \right\} \\ & + \frac{n\alpha_2}{(3n-2)} + \frac{\alpha_1(n-2+2v_1/x)}{(3n-2)} \\ & - \frac{\alpha_2 v'_2}{(3n-2)\kappa} - \frac{\alpha'_2 v_2}{(3n-2)\kappa} + \frac{nx\alpha'_2}{(3n-2)}. \end{aligned} \quad (E8)$$

We can then readily solve for the two eigenvalues of  $v'_1(x)$ , corresponding two eigendirections. The two possible eigendirections across the corresponding sonic critical curve of fluid 2 can be computed in the same manner.

## APPENDIX F: SHOCK CONDITIONS

As stated in subsection of self-similar shocks 2.6, all variables with subscript  $\{u, i\}$  refer to variables on the upstream side of a shock for fluid  $i$ , while all variables with subscript  $\{d, i\}$  refer to variables on the downstream side of a shock for fluid  $i$ . Convenient variables  $\Gamma_{u,i}$  and  $\Gamma_{d,i}$  are defined by

$$\Gamma_{d,i} \equiv n - \frac{v_{d,i}}{x_{d,i}}, \quad (F1)$$

$$\Gamma_{u,i} \equiv n - \frac{v_{u,i}}{x_{u,i}}. \quad (F2)$$

Parameter  $\lambda_i$  defined by

$$\lambda_i = \left( \frac{K_{d,i}}{K_{u,i}} \right)^{1/2} \quad (F3)$$

is essentially the sound speed ratio of downstream and upstream sides of a shock and should be greater than 1 for entropy increase on the downstream side. According to the dimensionless equation of state (see equation (8)), the dimensional equation of state is

$$P_i = K_i^{(1-3q_i/2)} (4\pi)^{\gamma_i-1} G^{\gamma_i-1+q_i} (3n-2)^{q_i} M_i^{q_i} \rho_i^{\gamma_i}. \quad (F4)$$

Then shock equations (equation of mass conservation, radial momentum conservation equation and energy conservation



equation (52)–(54) can be rearranged into dimensionless self-similar forms of

$$\begin{aligned} \alpha_{u,i}(nx_{u,i} - v_{u,i}) &= \alpha_{d,i}(nx_{d,i} - \lambda_i v_{d,i}) \\ &= \alpha_{d,i} \lambda_i (nx_{d,i} - v_{d,i}), \end{aligned} \quad (\text{F5})$$

$$\begin{aligned} \lambda_i^2 \left[ \alpha_{d,i}^{q_i+\gamma_i} x_{d,i}^{2q_i} (nx_{d,i} - v_{d,i})^{q_i} + \alpha_{d,i} (nx_{d,i} - v_{d,i})^2 \right] \\ = \alpha_{u,i}^{q_i+\gamma_i} x_{u,i}^{2q_i} (nx_{u,i} - v_{u,i})^{q_i} + \alpha_{u,i} (nx_{u,i} - v_{u,i})^2, \end{aligned} \quad (\text{F6})$$

$$\begin{aligned} \lambda_i^2 \left[ \frac{(nx_{d,i} - v_{d,i})^2}{2} + \frac{\gamma_i \alpha_{d,i}^{q_i+\gamma_i-1}}{(\gamma_i-1)} x_{d,i}^{2q_i} (nx_{d,i} - v_{d,i})^{q_i} \right] \\ = (nx_{u,i} - v_{u,i})^2/2 \\ + \gamma_i \alpha_{u,i}^{q_i+\gamma_i-1} x_{u,i}^{2q_i} (nx_{u,i} - v_{u,i})^{q_i} / (\gamma_i - 1). \end{aligned} \quad (\text{F7})$$

With  $\Gamma_1$  and  $\Gamma_2$  for the two coupled fluids, we can rewrite the above three equations in more symmetric forms, namely

$$\alpha_{u,i} \Gamma_{u,i} = \alpha_{d,i} \Gamma_{d,i}, \quad (\text{F8})$$

$$\begin{aligned} \alpha_{d,i}^{q_i+\gamma_i} x_{d,i}^{3q_i-2} \Gamma_{d,i}^{q_i} + \alpha_{d,i} \Gamma_{d,i}^2 \\ = \alpha_{u,i}^{q_i+\gamma_i} x_{u,i}^{3q_i-2} \Gamma_{u,i}^{q_i} + \alpha_{u,i} \Gamma_{u,i}^2, \end{aligned} \quad (\text{F9})$$

$$\begin{aligned} \frac{\Gamma_{d,i}^2}{2} + \frac{\gamma_i}{(\gamma_i-1)} \alpha_{d,i}^{q_i+\gamma_i-1} x_{d,i}^{3q_i-2} \Gamma_{d,i}^{q_i} \\ = \frac{\Gamma_{u,i}^2}{2} + \frac{\gamma_i}{(\gamma_i-1)} \alpha_{u,i}^{q_i+\gamma_i-1} x_{u,i}^{3q_i-2} \Gamma_{u,i}^{q_i}. \end{aligned} \quad (\text{F10})$$

From above three equations (F8)–(F10),  $\Gamma_{u,i}$  upstream of a shock can be determined by the variables on the downstream side of a shock from the following quadratic equation

$$\begin{aligned} \frac{(\gamma_i+1)}{2\gamma_i} \Gamma_{u,i}^2 - \left( \alpha_{d,i}^{q_i+\gamma_i-1} \Gamma_{d,i}^{q_i-1} x_{d,i}^{3q_i-2} + \Gamma_{d,i} \right) \Gamma_{u,i} \\ + \alpha_{d,i}^{q_i+\gamma_i-1} \Gamma_{d,i}^{q_i} x_{d,i}^{3q_i-2} + \frac{(\gamma_i-1)}{2\gamma_i} \Gamma_{d,i}^2 = 0, \end{aligned} \quad (\text{F11})$$

where subscript  $i = 1, 2$  correspond to fluid 1 and 2, respectively. One root of quadratic equation (F11) is a trivial solution  $\Gamma_{u,i} = \Gamma_{d,i}$ , which is omitted. The other root of physical relevance is given in the subsection of self-similar shocks 2.6.

## APPENDIX G: SOUND SPEED RATIO

In our two-fluid model framework, the velocity dispersion of dark matter particles (DMPs) is mimicked by an equivalent ‘sound speed’. This velocity dispersion of DMPs produces a pressure-like effect. In this scenario, the polytropic sound speed for fluid  $i$  is given by

$$a_i = \left( \frac{\partial P_i}{\partial \rho_i} \right)_s^{1/2} = \left( \frac{\gamma_i P_i}{\rho_i} \right)^{1/2}. \quad (\text{G1})$$

By self-similar transformation (5), this polytropic sound speed can be written as

$$a_i = \left( \gamma_i \frac{\beta_i}{\alpha_i} \right)^{1/2} K_i^{1/2} t^{n-1}. \quad (\text{G2})$$

As the reduced pressure  $\beta_i$  is determined by the reduced equation of state (8) and there is an expression (6) for the

reduced enclosed mass, the polytropic sound speed in fluid  $i$  can be written as

$$a_i = \gamma_i^{1/2} K_i^{1/2} t^{n-1} \alpha_i^{(q_i+\gamma_i-1)/2} x_i^{q_i} (nx_i - v_i)^{q_i/2}. \quad (\text{G3})$$

Since  $(K_1/K_2)^{1/2} = x_2/x_1 = \kappa$ , the sound speed ratio of fluid 1 to fluid 2 is given by

$$\frac{a_1}{a_2} = \left( \frac{\gamma_1}{\gamma_2} \right)^{1/2} \kappa^{1-q_2} \frac{\alpha_1^{(q_1+\gamma_1-1)/2}}{\alpha_2^{(q_2+\gamma_2-1)/2}} x^{q_1-q_2} \frac{(nx_1 - v_1)^{q_1/2}}{(nx_2 - v_2)^{q_2/2}}. \quad (\text{G4})$$

The sound speed varies with radius and the sound speed ratio at different radii can be computed according to equation (G4).

In the regime of  $x \rightarrow 0^+$ , we take the quasi-static solution of our model and the asymptotic behaviour of density is determined by equation (25) (velocities are small compared with  $x$ ). Thus when  $x \rightarrow 0^+$ , the sound speed ratio has the asymptotic behaviour

$$\frac{a_1}{a_2} \rightarrow \left( \frac{\gamma_1}{\gamma_2} \right)^{1/2} \kappa^{1-3q_2/2} \frac{A_1^{(q_1+\gamma_1-1)/2}}{A_2^{(q_2+\gamma_2-1)/2}}. \quad (\text{G5})$$

As the coefficients of static polytropic solution  $A_1$  and  $A_2$  are determined by equation (18), the sound speed ratio at small radius is

$$\frac{a_1}{a_2} = \left( \frac{\gamma_1}{\gamma_2} \frac{n^{q_2}}{n^{q_1}} \right)^{1/2}. \quad (\text{G6})$$

Therefore in the limit of  $x \rightarrow 0^+$  and for the quasi-static solution, the sound speed ratio is independent of  $\kappa$  and is only dependent on  $n$  and on the two polytropic indices  $\gamma_i$ .

In the limit of  $x \rightarrow +\infty$ , the asymptotic behaviour of density is determined by equation (28) and equation (29) (velocities are small compared with  $x$ ), so the asymptotic behaviour of sound speed ratio at large  $x$  is

$$\frac{a_1}{a_2} \rightarrow \left( \frac{\gamma_1}{\gamma_2} \right)^{1/2} \kappa^{1-3q_2/2} \frac{E_1^{(q_1+\gamma_1-1)/2}}{E_2^{(q_2+\gamma_2-1)/2}}, \quad (\text{G7})$$

where  $E_1$  and  $E_2$  are two coefficients determined by equations (28) and (29).

Two specific examples for the radial profile of polytropic sound speed ratio  $a_2/a_1$  are shown in Fig. 6 and Fig. 15 in the main text.

## REFERENCES

- Bagchi J., Ensslin T. A., Miniati F., Stalin C. S., Singh M., Raychaudhury S., Humeshkar N. B., 2002, *New Astron.*, 7, 249
- Bagchi J., Durret F., Gastão B. L. N., Paul S., 2006, *Science*, 314, 791
- Bahcall N. A., 1996 (astro-ph/9611148)
- Bertschinger E., 1989, *ApJ*, 340, 666
- Bertschinger E., 1998, *ARA&A*, 36, 599
- Bian F. Y., Lou Y. Q., 2005, *MNRAS*, 363, 1315
- Blanton E. L., Craig L. S., McNamara B. R., Michael W. W., 2001, *ApJ*, 558, L15
- Carilli C. L., Taylor B., 2002, *ARA&A*, 40, 319
- Carlson E. L., Machacek M. E., Hall L. J., 1992, *ApJ*, 198, 43
- Cavaliere A., Fusco-Femiano R., 1976, *A&A*, 49, 137

- Cavaliere A., Fusco-Femiano R., 1978, *A&A* 70, 677
- Cen R., Ostriker J. P., 1999, *ApJ*, 514, 1
- Cen R., Ostriker J. P., 2006, *ApJ*, 650, 560
- Churazov E., Forman W., Jones C., Böhringer H., 2003, *ApJ*, 590, 225
- Clowe D., Bradac M., Gonzalez A. H., et al., 2006, *ApJ*, 648, L109
- Ensslin T. A., Biermann P. L., Klein U., Kohle S., 1998, *A&A*, 332, 395
- Ettori S., 2003, *MNRAS*, 344, L13
- Ettori S., Fabian A. C., 1999, *MNRAS*, 305, 834
- Evrard A. E., 1990, *ApJ*, 363, 349
- Evrard A. E., Summers F. J., Davis M., 1994, *ApJ*, 422, 11
- Fabian A. C., 1994, *Annu. Rev. Astron. Astrophys.*, 32, 277
- Fabian A. C., Sanders J. S., Allen S. W., Crawford C. S., Iwasawa K., Johnstone R. M., Schmidt R. W., Taylor G. B., 2003, *MNRAS*, 344, L43
- Fabian A. C., Sanders J. S., Taylor G. B., Allen S. W., Crawford C. S., Johnstone R. M., Iwasawa K., 2006, *MNRAS*, 366(2), 417
- Fatuzzo M., Adams F. C., Myers P. C., 2004, *ApJ*, 615, 813
- Freedman W. L., et al. 2001, *ApJ*, 553, 47
- Frenk C. S., Evrard A. E., White S. D. M., Summers F. J., 1996, *ApJ*, 472, 460
- Gabici S., Blasi P., 2003, *ApJ*, 583, 695
- Gizani N. A. B., Leahy J. P., 2004, *MNRAS*, 350, 865
- Goldreich P., Weber S. V., *ApJ*, 1980, 238, 991
- Gunn J. E., Gott J. R., 1972, *ApJ*, 176, 1
- Harris W. E., Racine R., 1979, *ARA&A*, 17, 241
- He P., Feng L. L., Fang L. Z., 2005, *ApJ*, 623, 601
- Hennawi J. F., Ostriker J. P., 2002, *ApJ*, 572, 41
- Hu J., Lou Y.-Q., 2004, *ApJ*, 606, L1
- Hu J., Shen Y., Lou Y.-Q., Zhang S.N., 2006, *MNRAS*, 365, 345 (astro-ph/0510222)
- Hu J., Lou Y.-Q., 2007, *MNRAS*, in press (2007arXiv:0711.3555)
- Hunter C., 1977, *ApJ*, 218, 834
- Jain B., Bertschinger E., 1996, *ApJ*, 456, 43
- Katz N., White S. D. M., 1993, *ApJ*, 412, 455
- Knebe A., Devriendt J. E. G., Mahmood A., Silk J., 2002, *MNRAS*, 329, 813
- Larson R. B., 1969a, *MNRAS*, 145, 271
- Larson R. B., 1969b, *MNRAS*, 145, 405
- Lea S. M., 1975, *Astrophys. Lett.*, 16, 141
- Lou Y. Q., 2005, *ChJAA*, 5, 6
- Lou Y.-Q., Cao Y., 2007, *MNRAS*, in press (2007arXiv:0711.1729)
- Lou Y. Q., Shen Y., 2004, *MNRAS*, 348, 717
- Lou Y. Q., Wang W. G., 2006, *MNRAS*, 372, 885
- Machacek M. E., 1994, *ApJ*, 431, 41
- Markevitch M. 1996, *ApJ*, 465, L1
- Markevitch M., Gonzalez A. H., David L., Vikhlinin A., Murray S., Forman W., Jones C., Tucker W., 2002, *ApJ*, 567, L27
- Markevitch M., Govoni F., Brunetti G., Jerius D., 2005, *ApJ*, 627, 733
- Markevitch M., Vikhlinin A., 2001, *ApJ*, 563, 95
- McGaugh S. S., 2007 (2007arXiv:0707.3795v1)
- McNamara B. R., Nulsen P. E. J., Wise M. W., Rafferty D. A., Carilli C., Sarazin C. L., Blanton E. L., 2005, *Nature*, 433, 45
- Mohayaee R. C., Shandarin S., Silk J., 2007 (2007arXiv:0704.1999v1)
- Moore B., Gelato S., Jenkins A., Pearce F. R., Quilis V., 2000, *ApJ*, 535, L21
- Natarajan V., Sikivie P., 2007 (2007arXiv:0711.1297v1)
- Navarro J. F., Frenk C. S., White S. D. M., 1996, *ApJ*, 462, 563
- Nulsen P. E. J., Hambrick D. C., McNamara B. R., Rafferty D., Birzan L., Wise M. W., David L. P., 2005, *ApJ*, 625, L9
- Nulsen P. E. J., McNamara B. R., Wise M. W., David L. P., 2005, *ApJ*, 628(2), 629
- Onemli V., Sikivie P., 2007 (2007arXiv:0710.4936v1)
- Ostriker J. P., 2000, *Phys. Rev. Lett.*, 84, 5258
- Peebles P. J. E., 2000, *ApJ*, 534, L127
- Peres C. B., Fabian A. C., Edge A. C., Allen S. W., Johnstone R. M., White D. A., 1998, *MNRAS*, 298, 416
- Penston M. V., 1969a, *MNRAS*, 144, 425
- Penston M. V., 1969b, *MNRAS*, 145, 457
- Press W. H., Flannery B. P., Teukolsky S. A., Vetterling W., 1986, *Numerical Recipes* (Cambridge University Press)
- Roettiger K., Burns J. O., Stone J. M., 1999, *ApJ*, 518, 603
- Rottgering H., Wieringa M. H., Hunstead R. W., Eckers R. D., 1997, *MNRAS*, 290, 577
- Sand D. J., Treu T., Smith G. P., Ellis R. S., 2003, *ApJ*, 604, 88
- Sanders J. S., Fabian A. C., 2006, *MNRAS*, 371, L65
- Sanders J. S., Fabian A. C., 2007 (2007arXiv:0705.2712v2)
- Sarazin C. L., Bahcall J., 1977, *ApJS*, 34, 451
- Sarazin C. L., 1988, *X-ray emission from clusters of galaxies*, Cambridge University Press, Cambridge
- Shchekinov Y. A., Vasiliev E. O., 2006, *MNRAS*, 368, 454
- Shu F. H., 1977, *ApJ*, 214, 488
- Silk J., Arons J., 1975, *ApJ*, 200, L131
- Spergel D. N., Steinhardt P. J., 2000, *PRL*, 84, 3760
- Spergel D. N., et al., 2003, *ApJS*, 148, 175
- Subramanian K., 2000, *ApJ*, 538, 517
- Suto Y., Silk J., 1998, *ApJ*, 326, 527
- Taylor G. B., Perley R. A., Inoue M., Kato T., Tabara H., Aizu K., 1990, *ApJ*, 360, 41
- Thomas P. A., Couchman H. M. P., 1992, *MNRAS*, 257, 11
- Tsai J. C., Hsu J. J. L., 1995, *ApJ*, 448, 774
- VandenBerg D. A., 1978, *ApJ*, 224, 394
- Verbunt F., van Paradijs J., Elson R., 1984, *MNRAS*, 210, 899
- Voit G. M., 2005, *Rev. Mod. Phys.*, 77, 207
- Wang W.-G., Lou Y.-Q., 2007, *ApSS*, 311, 363 (2007arXiv:0706.3959W)
- Whitworth A., Summers D., 1985, *MNRAS*, 214, 1
- Yahil A., 1983, *ApJ*, 265, 1047
- Yahil A., Ostriker J. P., 1973, *ApJ*, 185, 787
- Yu C., Lou Y.-Q., Bian F. Y., Wu Y., 2006, *MNRAS*, 370, 121